The electrochemical interface in first-principles calculations

Kathleen Schwarz

Material Measurement Laboratory, National Institute of Standards and Technology, 100 Bureau Dr., Gaithersburg, Maryland 20899, USA

Ravishankar Sundararaman

Department of Materials Science and Engineering, Rensselaer Polytechnic Institute, 110 8th St., Troy, New York 12180, USA

Abstract

First-principles predictions play an important role in understanding chemistry at the electrochemical interface. Electronic structure calculations are straightforward for vacuum interfaces, but do not easily account for the interfacial fields and solvation that fundamentally change the nature of electrochemical reactions. Prevalent techniques for first-principles prediction of electrochemical processes range from expensive explicit solvation using *ab initio* molecular dynamics, through a hierarchy of continuum solvation techniques, to neglecting solvation and interfacial field effects entirely. Currently, no single approach reliably captures all relevant effects of the electrochemical double layer in first-principles calculations.

This review systematically lays out the relation between all major approaches to first-principles electrochemistry, including the key approximations and their consequences for accuracy and computational cost. Focusing on *ab initio* methods for thermodynamic properties of aqueous interfaces, we first outline general considerations for modeling electrochemical interfaces, including solvent and electrolyte dynamics and electrification. We then present the specifics of various explicit and implicit models of the solvent and electrolyte. Finally, we discuss the compromise between computational efficiency and accuracy, and identify key outstanding challenges and future opportunities in the wide range of techniques for first-principles electrochemistry.

Keywords: Electrochemistry, Density-functional theory, Continuum solvation

Contents

Abbreviations and Symbols

DFT	Density Functional Theory
PCM	Polarizable Continuum Model
GCS	Gouy-Chapman-Stern
CHE	Computational Hydrogen Electrode
SHE	Standard Hydrogen Electrode
AIMD	*Ab initio* molecular dynamics
QM/MM	Quantum Mechanics/Molecular Mechanics
mPB	Modified Poisson Boltzmann
μ_e	Electron chemical potential
Φ	Grand free energy
A	Helmholtz free energy
C	Differential capacitance
k_BT	Thermal energy at temperature T
N_e	Number of electrons
ϕ	Electrode potential
ϕ_0	Potential of zero charge
σ	Surface charge density
E_z	Electric field normal to surface
ϵ_o	Dielectric permittivity of vacuum
ϵ_b	Relative permittivity of bulk material

1. Introduction

1.1. Motivation and Scope

The electrochemical environment strongly affects reactions at the electrochemical interface. Precise control of electrochemical processes, from energy conversion and storage [1, 2], to electrochemical wastewater treatment [3–5], corrosion [6], and electrodeposition [7], relies on understanding and manipulating the properties of the double layer region. Computational design of new materials for these applications requires an accurate description of both chemical interactions from first-principles calculations and the effects of the electrochemical environment. For instance, the effects of ion solvation, electrolyte bonding, *and* potential at the solid-electrolyte interface must be considered when designing energy materials with increased operating voltage windows and energy storage capacity [8]

Capturing the effects of the electrochemical interface in first-principles calculations remains challenging [9, 10]. Techniques to account for solvation and electrification in first-principles electrochemistry vary considerably in level of detail, accuracy and computational expense, and cross over many disciplines. There is not yet a coherent overview of all these techniques with a clear comparison of which physical and chemical effects they each account for, making it difficult for practitioners in this field to choose the appropriate technique for their investigation. In particular, continuum solvation models have developed significantly in recent years and are capable of inexpensively describing an increasing number of solvation effects in electrochemistry [11–18]. However, the appropriateness of these models for describing any given electrochemical phenomena is not yet widely known beyond the solvation model development community, limiting the application of recent and more advanced models.

In this review, we seek to help researchers applying first-principles methods to electrochemical systems understand the state of available techniques, ranging from expensive first-principles molecular dynamics to inexpensive implicit solvation models, and guide their selection of the most appropriate modeling approach. We also aim to provide a broad understanding of the outstanding issues associated with solvation model development for electrochemistry, targeting model developers and practitioners from diverse fields. Thus, we limit our focus to calculations of aqueous, charged interfaces using periodic density-functional theory, with emphasis on the *range of calculation techniques*, versus specific application to chemical problems, reaction mechanisms, or kinetics.

This article begins by explaining the crucial differences between ultra-high vacuum surface science and electrochemistry and the complex, nonlinear interfacial properties that arise due to the charge on the electrode. We thus motivate the need for models of the electrochemical double layer, provide an overview of such approaches, and discuss general considerations for first-principles electrochemistry that span all these approaches. We then describe approaches that use explicit solvent and/or electrolyte atoms to describe the interface, followed by continuum solvation approaches in the final section.

1.2. Electrochemical interfaces

Electrochemistry and vacuum surface science both focus on interfacial properties that depend on surface potentials and adsorbate coverage. [19]. However, electrochemistry differs fundamentally from *surface science in an electrolyte.*

The key difference arises from the capability of mobile charges (ions) in the electrolyte to balance charges on the electrode, forming the electric double layer that localizes electric fields to the immediate vicinity of the electrode surface [20]. This makes it possible for the electrode surface and adsorbates at the surface to easily adopt charged states, rapidly equilibrating electrons with the bulk electrode and ions with the bulk electrolyte. Further, equilibrium charge states of each possible atomic configuration of the interface change with electrode potential, making properties of the electrochemical interface strongly potential dependent. Consequently, the most convenient description of electrochemical interfaces uses the grand canonical ensemble with respect to both electrons and electrolyte ions, with the bulk electrode and electrolyte serving as the corresponding reservoirs.[1] In con-

Email addresses: kas4@nist.gov (Kathleen Schwarz), sundar@rpi.edu (Ravishankar Sundararaman)

[1] The bulk regions are reservoirs by definition when the interfacial region is the system chosen for defining the thermodynamic ensemble.

trast, the canonical ensemble is the most convenient description of constant-charge vacuum interfaces. This fundamental difference between vacuum and electrochemical interfaces [21] necessitates drastically different approaches for first-principles electrochemistry [22].

The chemical potential μ_e of electrons is a key thermodynamic parameter that governs this grand canonical ensemble, and is closely related – equivalent up to an offset as we discuss in Section 2.1 – to the electrode potential. This chemical potential directly influences the grand free energy $\Phi \equiv A - N_e\mu_e$, where A is the Helmholtz free energy and N_e is the total number of electrons. Further, Φ is the thermodynamic quantity minimized in equilibrium in this ensemble and is therefore the key quantity of interest in determining electrochemical reaction pathways. The lowest order effect of μ_e is that it linearly alters the free energy Φ with a slope that depends on the charge state (related to N_e). The earliest first-principles schemes for predicting electrode properties [23] and electrochemical reaction mechanisms [24–26] employed this approximation of a linear relationship between Φ and μ_e, neglecting deviations from integer charge states and corresponding changes in the Helmholtz free energy.

However, the potential (μ_e) does not alter the thermodynamics of the electrochemical interface in this strictly linear manner. Changing μ_e necessarily results in a corresponding change of the local charge at the electrode surface, and hence N_e as well. This charge, in turn, generates a local electric field $\vec{E}(\vec{r})$ at the surface of the electrode, which affects the free energy, A, that may critically impact reaction mechanisms and rates [27–30]. In particular, the interaction of the induced dipole moments of the adsorbates with the local electric fields and electrostatic interactions with the surface can introduce a nonlinear change in the energies with field [31–33]. The net result is a complex nonlinear variation of charges, fields and free energies in response to the electrode potential, which are all sensitive to the structure and electric response of the electrochemical interface.

Figure 1 schematically illustrates this key difference between the role of the potential in vacuum and electrochemical interfaces. In vacuum (Figure 1(a)), the potential is applied relative to another electrode far away, and the electric field at the surface depends on the separation between these electrodes and their overall geometry. The surface charge density at the electrode is proportional to the surface electric field by Gauss's law, $\sigma = \epsilon_0 E_z$, and the counter charge appears only on the other electrode, so that the electric field does not vary spatially at the atomic scale. The electrode potential (or potential difference to the other electrode) in vacuum is not physically significant: only this surface electric field influences the energetics of processes at the vacuum interface [35]. Consequently, first-principles calculations sometimes apply uniform electric fields like those shown in Figure 1(a) to approximate the complex field effects in electrochemical interfaces [27].

The electrolyte dramatically changes this picture (Figure 1(b)) due to its solvated ionic charges that can move in response to the field. The ions balance the charge on the electrode such that the net charge up to a distance z into the electrolyte decays exponentially, and then by Gauss's law, so does the electric field $E_z(z)$. [2] Most importantly, this makes the local electric field distribution and charge density depend only on the electrode potential, and not on the overall geometry up to the far away counter-electrode (not shown) in the electrochemical cell. The same potential difference results in fields localized to a much smaller length scale than the vacuum case, resulting in much larger electric fields near the electrode surface, and correspondingly, much larger surface charge densities. Additionally, the solvent in the electrolyte also exhibits a dielectric response which further enhances the surface charge density, $\sigma = \epsilon_b E_z$, since the dielectric permittivity $\epsilon_b \gg \epsilon_0$ for most solvents used in electrochemistry. (For example, $\epsilon_b \approx 80\epsilon_0$ for liquid water at standard conditions.) Consequently, electric fields are typically much larger at electrochemical interfaces than their vacuum counterparts, resulting

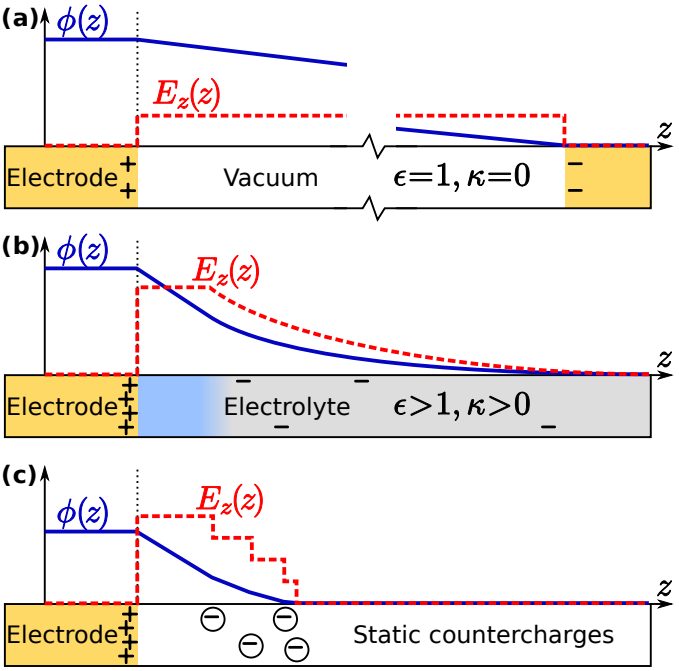

Figure 1: Schematic comparison of electrostatic potentials ϕ and electric fields $\vec{E}$ in (a) vacuum between a *pair of electrodes*, (b) in an electrode-electrolyte interface (for simplicity, sketched using the Gouy-Chapman-Stern model [34]) and (c) with a fixed configuration of counter charges. For equal potential differences, Debye screening with inverse-length κ in (b) localizes fields within a half cell and increases capacitance relative to (a). For equal surface charge density generating the same surface field, static counter charges do not generally capture the thermodynamically-averaged field distribution, potential and capacitance.

[2] As the net charge approaches zero, the potential asymptotes to the potential of the electrons deep in the fluid, which is solely a property of the bulk electrolyte; the reference potential of an electron in that electrolyte.

in substantially larger electrification effects.[3] Experimentally, these surface electric fields are often characterized using Stark shifts in vibrational frequencies of adsorbates [36–39], but the interpretation of these experiments requires careful description of the charge and electric field distribution in the double layer [40, 41].

This schematic picture of the potential and electric field distribution is the essence of the classical Gouy-Chapman-Stern model of the electrochemical interface: the electrode surface is adjacent to the solvent (dielectric) component of the electrolyte in a region that excludes ions due to their larger effective size, and the ions distribute exponentially outside this region [34, 42]. The dimensions and dielectric response of the solvent region, and the precise ionic distribution beyond, all contribute significantly in determining the relationship between the electrode potential, surface charge density, and electric field distributions. First-principles calculations that attempt to account for the local electrification of the electrode surface often employ fixed ions as counter-charges [43, 44] to mimic the electrolyte charge density (Figure 1(c)). This approach can introduce surface electric fields by controlling the counter-charge surface density, but neglecting dynamics prevents, in general, simultaneously capturing realistic potential, electric field and charge distributions within the electrochemical interface.

1.3. Electrochemical capacitance

The charge density $\sigma(\phi)$ on an electrode surface at a given potential ϕ is determined by both the potential at which the electrode surface is neutral, *i.e.*, the potential of zero charge, $\sigma(\phi_0) = 0$, and the electrochemical capacitance. The potential of zero charge is related to the energy required to move an electron from the electrode to the bulk electrolyte, up to a constant offset in the experimental potential scale that arises from the reference electrode potential [45].[4] It is analogous to the work function of a surface in vacuum, defined as the energy required to move an electron from the surface to the vacuum, but the potential of zero charge additionally includes solvation effects.

The variation of charge with potential is captured by the differential capacitance, $C(\phi) = \mathrm{d}\sigma(\phi)/\mathrm{d}\phi$, defined per unit area of the interface. Integrating from the potential of zero charge, the electrode surface charge density at any potential[5] is given by $\sigma(\phi) = \int_{\phi_0}^{\phi} \mathrm{d}\phi' C(\phi')$. The electrochemical capacitance quantifies the relationship between the net potential across the entire electrochemical interface and the (equal and opposite) charge on each side of it. It does not directly capture the microscopic charge, field and potential distributions discussed above. However, its dependence on potential and electrolyte concentration provides indirect information about the contributions from various spatial regions within the electrochemical interface.

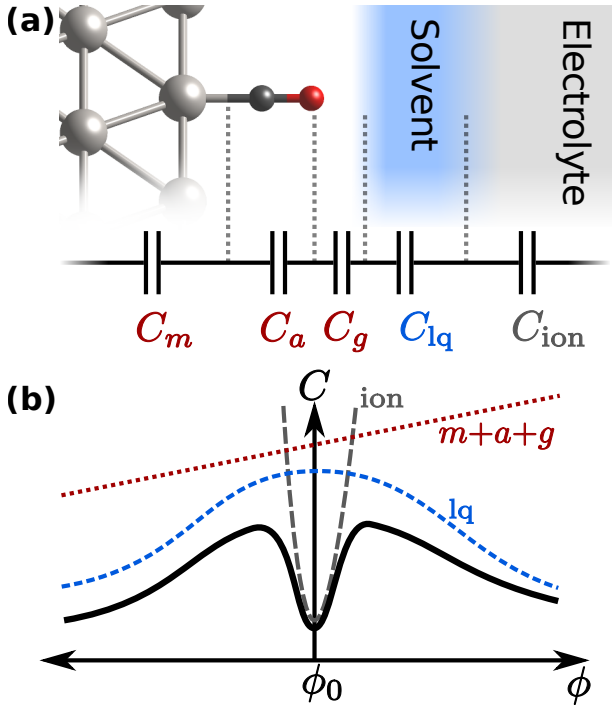

Figure 2: (a) Schematic spatial decomposition of electrochemical capacitance of Pt(111) with adsorbed CO into metal (quantum, C_m), adsorbate (C_a), gap (C_g), solvent (C_{lq}) and ionic (C_{ion}) capacitances in series, and (b) their typical corresponding dependencies on electrode potential. (Adapted with permission from Ref. 40.)

Figure. 2(a) shows a simple idealized model for electrochemical capacitance that generalizes the classical Gouy-Chapman-Stern (GCS) model and assumes that the electrochemical interface can be decomposed into distinct spatial regions with precisely defined charges. A sequence of (approximately) neutral regions separate the electrode region with surface charge density σ from the electrolyte region with surface charge density $-\sigma$ (integrated over the z-extent of the electrolyte).[6] The original GCS model [34, 42] assumes a single neutral region corresponding to the solvent alone, but realistic electrochemical interfaces also include a 'gap' region with no dielectric response between the solvent and the electrode (where the electron density of each is negligible), and optionally, adsorbates on the electrode forming an additional dielectric layer [40].

Within this simple model, the electric field in each intermediate region is directly determined by σ using Gauss's

[3] Note that the electric field is screened substantially by the dielectric response of the solvent within the solvent and electrolyte regions. However, the surface of the solvent is still subjected to the large unscreened surface electric fields, and these fields determine the response of the solvent.

[4] Here, we define the potential of zero charge of a surface without adsorbates. In the presence of adsorbates, the PZC depends on the charge transferred to the electrode, and hence is not intrinsic to solely the metal electrode [46].

[5] This assumes no irreversible reduction or oxidation reactions.

[6] The intermediate regions may only be approximately neutral, accounting for finite electron density (or spill-over) in the gap region and small but non-zero probabilities of ions in the liquid region.

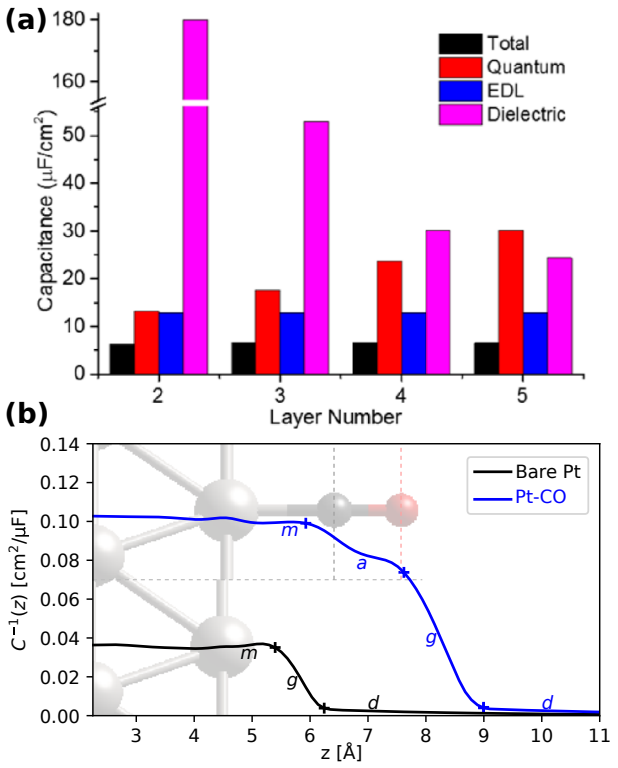

Figure 3: (a) Total capacitance is dominated by quantum capacitance rather than the electrochemical double layer (EDL) or dielectric contributions for few-layer graphene electrodes [47], and (b) by the adsorbate and gap (a, g) capacitances in CO adsorbed on Pt electrodes rather than the metal or diffuse (m, d) capacitances [40]. (Adapted with permission from Refs. 40 and 47.)

law, $E = \sigma/\epsilon(E)$, where $\epsilon(E)$ is the permittivity of that region, which could depend on the electric field (nonlinear response). This in turn directly determines the potential difference, $\phi = \sigma w/\epsilon(E)$, where w is the thickness of that region, and hence the differential capacitance, $C(E) = \mathrm{d}\sigma/\mathrm{d}\phi = (\epsilon(E) + E\epsilon'(E))/w$. The two end regions, the metal and the electrolyte, each generate a surface charge density that depends directly on the potential ϕ in that region. The net potential difference across the entire interface is the sum of the potential differences in each region, each forming a capacitor with the same surface charge density σ. Therefore, the net electrochemical capacitance is nominally the series combination of differential capacitances in each spatial region shown in Figure. 2(b), $C_{\mathrm{net}}^{-1} = C_m^{-1} + C_a^{-1} + C_g^{-1} + C_{\mathrm{lq}}^{-1} + C_{\mathrm{ion}}^{-1}$.

The differential capacitance of each neutral region above could depend nonlinearly on the field, while the differential capacitance of each charged region could depend nonlinearly on the potential. Therefore calculating the overall capacitance involves non-trivial coupled equations that require numerical solution in general. [7] The series capacitor model still serves as a useful first approximation, with the primary consequence that the net capacitance is dominated by the *smallest capacitance* in series. For example, the 'quantum' capacitance of the electrode $C_m(\phi) = e^2 w g(\varepsilon_F(\phi))$, where w is the thickness of the electrode and $g(\varepsilon_F(\phi))$ is the electronic density of states at the Fermi level at a given electrode potential ϕ, is extremely large for conventional metallic electrodes and therefore negligible. In contrast, two-dimensional electrodes such as graphene and 2D boron can have a low quantum capacitance which can dominate the overall electrochemical capacitance [47, 49]. For example, Figure 3(a) shows that with decreasing number of layers in few-layer graphene electrodes, the quantum capacitance decreases proportionally and limits the total capacitance, even though the dielectric capacitance (C_{lq}) increases [47].

Similarly, adsorbates on the electrode surface *e.g.,* CO on a Pt electrode, can introduce a dielectric layer C_a with a low capacitance that can dominate the overall capacitance; this is sometimes grouped together with the electrode, resulting in a low quantum capacitance for electrode + adsorbate. This presents challenges for experimental probes of local electric fields, such as Stark shifts of the vibrational resonances of adsorbates (such as CO), because the introduction of adsorbates can drastically alter the field distribution by changing the dominant lowest capacitor [40]. Further, hydrophobic adsorbates could even strongly reduce the adjacent gap capacitance (discussed in Figure 2), making that the dominant contribution instead. For example, CO adlayers on Pt electrodes decrease the total capacitance both by introducing an adsorbate capacitance C_a and by reducing the gap capacitance C_g [40], as shown in terms of the inverse capacitance (potential profile divided by charge on the electrode) in Figure 3(b). Additionally, the changing local electric field with charge can alter the adsorbate geometry, such as in the case of Cl, Br adlayers adsorbed on Cu(100) [50, 51], which can result in nonlinear changes of the quantum (or adsorbate-layer) capacitance with electrode potential.

The gap region is typically very narrow ($\ll 1$ Å), but can have a relatively small capacitance (large impact on total capacitance) due to its low dielectric constant (≈ 1). In addition to adsorbates as discussed above, the gap capacitance can also change with potential as the location of the charge responses in the electrode and solvent can vary with the applied potential (and corresponding local electric field). In principle, the electrode and solvent need not even exhibit the strict charge separation assumed above, as electrons may weakly delocalize across the interface, and chemical interactions leading to charge transfer can occur between the electrode and solvent. The impact of such 'charge spillover' into the fluid is still not completely known and remains the subject of active research [52–56].

The region to the right of the gap in Figure 2(a) consisting of solvent and electrolyte ions is the portion captured by the Gouy-Chapman-Stern model. The ionic capacitance increases strongly with magnitude of potential

[7] Approximating this complex capacitance behavior at the interface as a constant [48] may suffice for modeling certain reactions at nearly neutral interfaces.

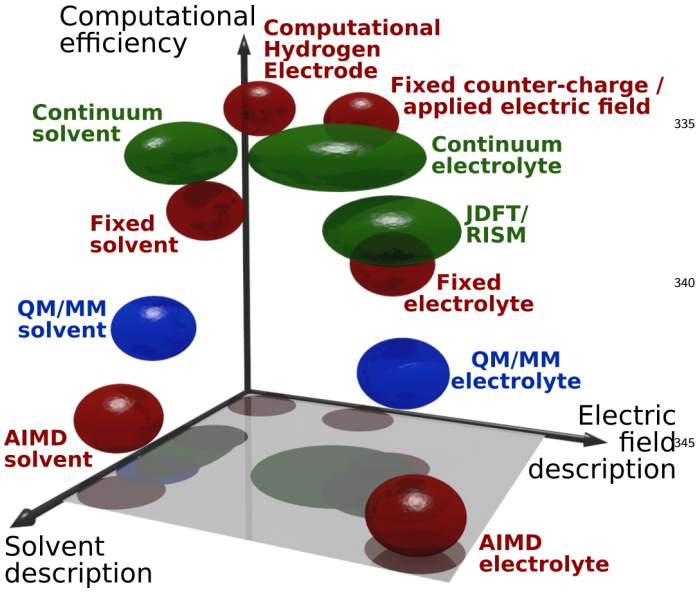

Figure 4: First-principles electrochemical simulations vary widely in accuracy of solvation effects, electric field distributions and computational efficiency. Pure DFT techniques (shown in red) may employ no solvent molecules / electrolyte ions, fixed configurations thereof, or full molecular dynamics (AIMD). Hybrid techniques can achieve significant gains in computational efficiency, including QM/MM approaches (shown in blue) that treat solvent/electrolyte atoms with force fields, and continuum approaches (shown in green) that treat solvents/electrolytes using density and charge distributions alone.

(Poisson-Boltzmann behavior), while the solvent capacitance decreases with magnitude of electric field (controlled by the potential) due to dielectric saturation, as discussed in detail below in Sections 4.1 and 4.5. The net series combination results in the characteristic shape of electrochemical capacitance variation with potential comprising a broad hump with a narrow dip near the potential of zero charge. Low values of quantum, adsorbate or gap capacitances in series would typically mask this shape, and therefore this shape is most often seen experimentally for inert metallic electrodes in non-adsorbing electrolytes. A goal of modern computational electrochemistry is to probe the local electric field effects in realistic electrochemical interfaces beyond the GCS regime, and to accurately predict the total charge on the electrode as well as microscopic charge and field distributions as a function of potential.

1.4. Overview of approaches

First-principles calculations of electrochemical systems must correctly capture the field and charge distributions in order to accurately predict the potential and electrolyte dependence of electrochemical processes. Because of the localization of the electric field, these calculations only need to describe an electrochemical half-cell: a single, charged electrode and its double layer.[8] Broadly, these calculations need electrification techniques to introduce charge on the surface (section 2.1) and dynamics to account for thermodynamic averaging of solvent and electrolyte configurations (section 2.2). These approaches classify into explicit solvation (section 3), where the solvent and electrolyte are included as atoms in the DFT or as classical atoms/molecules treated using force fields, and implicit solvation (section 4) which approximates only the density or distribution of solvent and/or electrolyte. Fig. 4 schematically outlines the most common approaches used in first-principles electrochemistry.

Fully explicit *ab initio* approaches treat the entire system using DFT or another quantum mechanical method. These include the simplest computational hydrogen electrode approaches [25] that do not include any solvent molecules or electrolyte ions. Introducing electric fields or counter-charges [27, 43] can improve the description of the electric field distribution (Fig. 4), but still neglect solvation effects. Frozen configurations of solvent molecules and electrolyte ions (section 3.1) can somewhat improve the description of solvation and electric field effects, but systematically capturing these effects in an explicit approach requires thermodynamic sampling over all possible configurations using a molecular dynamics approach.

Molecular dynamics simulations of solvent and electrolytes are potentially the most accurate technique for first-principles electrochemistry, but incur significant computational cost both due to the large number of additional atoms included within the quantum-mechanical DFT calculation and the large number of atomic configurations that must be calculated explicitly. Hybrid quantum mechanics / molecular mechanics (QM/MM) methods (section 3.3) can relieve the number of atoms in DFT compared to full *ab initio* molecular dynamics (AIMD) calculations (section 3.2), but still require calculation of a large number of configurations. Most importantly, the length scales of ion distributions in an electrolyte (especially at low concentrations) and the time scales of equilibration of this distribution make both the system size and number of configurations extremely large for molecular dynamics treatment of electrochemical interfaces [57–59].

Implicit solvation methods (section 4) replace explicit solvent molecules or electrolyte atoms with continuum approximations of their densities and charge distributions. These distributions are implicitly averaged over all possible configurations, removing the need for thermodynamic sampling, making these techniques highly efficient computationally. Recent developments in implicit solvation models capture an increasing level of detail in the response of the electrolyte, potentially achieving an accurate description of solvation and electric field effects at low computational cost (Fig. 4).

Another way to classify these approaches is into 'pure' approaches that treat every atom with the same theory, and hybrid techniques. AIMD is arguably the only pure approach, while both implicit solvation models and QM/MM are hybrid techniques that contain regions of quantum de-

[8] Additionally, the difference in chemical potential of the electrons at two half-cells in an electrochemical cell prevents a typical electronically equilibrated first-principles calculation from describing the full cell.

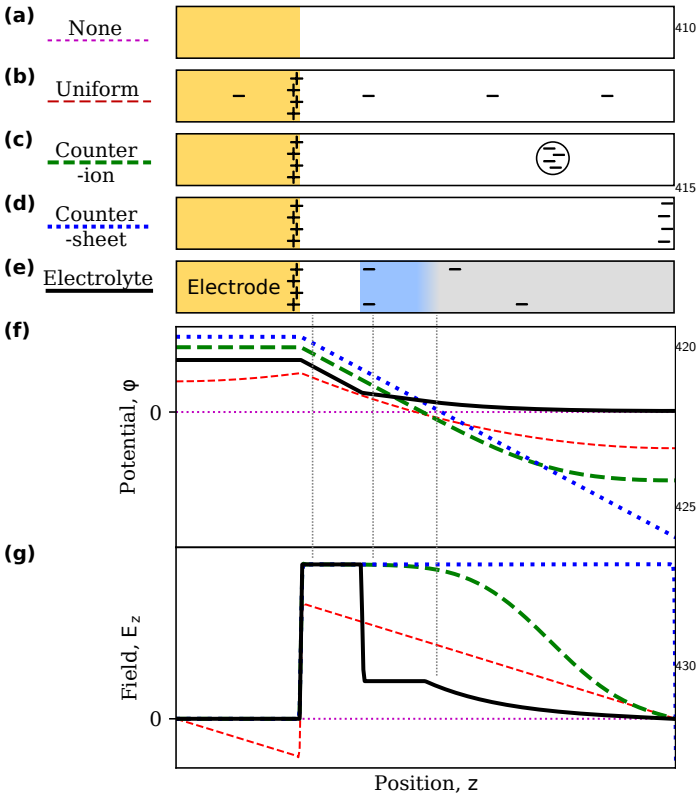

Figure 5: Schematic charge distributions in various approaches to electrification of a perfect metallic electrode, including (a) No electrification, various static counter-charge distributions such as (b) uniform compensating background, (c) static ions or (d) compensating charge layer / boundary condition, and (e) self-consistent counter-charge distribution in an electrolyte. (f) Corresponding electrostatic potentials and (g) electric fields in one half of an inversion-symmetric unit cell for a periodic calculation.

scription (using DFT) spatially separated from regions treated classically. The accuracy and reliability of the hybrid methods are often dependent on the treatment of this interfacial region. This requires careful matching between force fields and explicit solvent/electrolyte atoms in QM/MM methods (section 3.3) and careful parameterization of the solvation cavity (section 4.2) in implicit continuum solvation methods.

2. General considerations

2.1. Electrification schemes

In addition to choices for treating solvation effects, techniques for first-principles electrochemistry vary substantially in their approach for describing the effect of electrode potential and local electric fields (as shown in Figure 4). These range from no electrification (as in the computational hydrogen electrode), electrification using static countercharge distributions, and self-consistent electrification accounting for charge distribution in the electrolyte. As we discuss below in detail, these approaches differ significantly in the effective distribution of electric fields and potential near the electrode surface (Fig. 5).

At the simplest end of the electrification spectrum, linear free energy relation approaches [23, 24] such as the most basic application of the computational hydrogen electrode [25] only deal with neutral configurations explicitly (Fig. 5(a)). These approaches then expand the free energy as a linear function of potential about the neutral reference point, as discussed in section 1.2. Going beyond this linear approximation requires electrification: the treatment of charged surface configurations in order to capture the change of local geometries and adsorbate configurations due to the surface charge and electric field.

In periodic DFT calculations, charged surface configurations require special treatment that neutralize the unit cell. This is because total energies and electrostatic potentials of charged unit cells are not well-defined (diverge to infinity). There are many approaches for constructing *neutral unit cells of charged surface configurations*, starting from a uniform compensating background (jellium) charge density at the simplest level [60]. This is the default handling of charged unit cells in plane-wave basis DFT calculations, which set the average value of the electrostatic potential to zero. As shown in Fig. 5(b), this results in a linear spatial variation of electric field and a corresponding quadratic variation of potential that differs markedly from those in a real electrolyte.

The potential profile from a uniform counter-charge distribution can be improved by strategically placing localized counter charges, either in the form of an explicit ion [43, 44, 61] (Fig. 5(c)) or as a sheet of continuum charge density (equivalently a counter-electrode boundary condition) [62–64] (Fig. 5(d)). Both options result in an electric field localized between the electrode surface and this counter-charge layer, with a linear potential variation within that region. Ultimately, the most realistic counter-charge distributions result from both explicit and implicit electrolyte models [65–67], combining a region with constant electric field and linear potential nearer to the electrode, with a region of exponentially decaying field and potential beyond it (Fig. 5(e)).

In summary, the electrification scheme determines the fidelity of the potential and electric field profiles relative to those created by the electrolyte, as illustrated by Fig. 5(f) and (g). The uniform countercharge approach generates a physically-incorrect non-zero electric field (and corresponding potential variation) within the metallic electrode due to the countercharge distribution that covers the entire unit cell including the metallic region. The counter-ion and counter-sheet generate the same electric field as the electrolyte in the vicinity of the electrode, but miss the screening due to the solvent and electrolyte regions. This leads to an overestimate of the potential difference between the electrode and the regions of the unit cell far from it. Importantly, only calculations with an electrolyte exhibit a potential that decays asymptotically to a constant, while all other schemes yield a potential whose unit cell average is zero.

Finally, we need to establish the connection between

electrified calculations at a specific surface charge and the corresponding electrode potential. This connection can be split into two required components: establishing an absolute scale of electron chemical potential in the DFT calculations, and connecting this DFT scale with the experimental scale of electrode potentials. In particular, calculations that include implicit or explicit electrolytes automatically have a meaningful absolute scale of electrode potential because the electrostatic potential exponentially decays to zero far from the electrode surface (Fig. 5(e)) [68]. All other electrification schemes have an undetermined offset in the electrostatic potential far from the electrode and require an additional step of subtracting this asymptotic potential in referencing the electron chemical potential to an absolute scale [60]. Referencing the electrostatic potential to zero far from the system additionally sets the reference for the eigenvalues in Kohn-Sham DFT. The corresponding occupation factors of the Kohn-Sham orbitals are Fermi functions of these eigenvalues. Thus, the electron chemical potential, which is equivalent to the Fermi energy of the interface [69], is also referenced to zero electrostatic potential at infinity.

After fixing the electrostatic potential reference, the theoretical electron chemical potential must be calibrated to the experimental electrode potential scale. Implicit solvation approaches typically base this calibration on computed and measured potentials of zero charge of single-crystal metal electrodes [70]. Explicit calculations either relate the work function of the solvated interface to that of the experimentally determined standard hydrogen potential [71–74], or calculate the value of an internal reference, such as the free energy of a proton [75]. See Ref. 45 for a detailed review of these approaches.

2.2. Dynamics

The equilibrium electric field distribution within the electrochemical interface is a critical component of first-principles electrochemistry, as discussed above. Ensuring appropriate distributions of solvent, electrolyte and surface species at the electrode is a general challenge in any approach for predicting electrochemical phenomena at or near equilibrium. Moreover, these equilibrium distributions should correspond to the grand canonical ensemble with respect to both electrons and electrolyte ions, as discussed in Section 1.2. We outline the key considerations for correctly sampling equilibrium distributions of the appropriate ensemble in electrochemical calculations below.

First consider a completely explicit treatment of solvent and electrolyte in a first-principles calculation, which, in principle, should provide the most accurate description of both solvation and electric field effects ('AIMD electrolyte' in Figure 4). This is extremely computationally expensive for two reasons. First, most electrolytes in experiment have low concentrations of ions. This necessitates large simulation cells with large numbers of solvent molecules to include a statistically significant number of ion pairs in the calculation cell [59]. For example, 1 mol/L of monovalent ions in water corresponds to 56 water molecules ($\sim$ 170 atoms) per ion pair, while 0.1 mol/L of ions corresponds to 556 water molecules ($\sim$ 1700 atoms) per ion pair. This is significantly larger than typical DFT calculations for catalysis that already include 100-200 electrode atoms (surface slab and adsorbate). Second, in such simulation cells, the diffusion time scales for ions to sample their equilibrium distribution may substantially exceed the few to tens of picosecond time scales practical for AIMD simulations [57, 58]. This motivates replacing several solvent molecules and electrolyte ions in DFT with classical versions instead in the hybrid quantum mechanics / molecular mechanics (QM/MM) methods. Alternatively, a portion of the DFT solvent and electrolyte may also be replaced with continuum solvation models in hybrid explicit-implicit approaches [76, 77].

Electrolyte ions are the primary contributor to both issues leading to the extreme computational expense for full explicit solvation discussed above. Hence, current practical approaches to explicit solvation in electrochemistry predominantly include only solvent molecules, with electrolyte species, if any, restricted to those in the vicinity of the electrode. As a result, such calculations do not automatically capture the correct long-range variation of electrostatic potential and need special handling for electrification scheme, as discussed above in section 2.1. The grand canonical ensemble for the electrons additionally imposes a fluctuating electron count in these simulations, which requires a potentiostat to maintain the correct ensemble [78, 79]. The fluctuation of electron number can have physical consequences, affecting the electronic coupling of adsorbates and electrodes, which is a current topic of research [80–82].

Implicit solvation approaches using continuum models directly approximate the equilibrium distributions of the solvent and electrolyte, and thereby do not always require explicit dynamics. However, the interfacial structure of the electrode may involve adsorbate configurations and coverages that change with potential. Sampling the ensemble of such configurations is also important for accurate electrochemical simulations, requiring statistical techniques such as cluster expansions to average over many possible configurations [83, 84]. Finally, all of the above approaches still require additional dynamics techniques to model reactions, ranging from simple and relatively inexpensive nudged elastic band for reactions in fully continuum electrolyte, to metadynamics for more complex reactions and explicit solvent and electrolyte.

3. Explicit solvation

Solvation effects in electrochemistry may be described using explicit solvent / electrolyte molecules or implicit models, as discussed above. This section describes explicit approaches in *ab initio* calculations, starting from the simplest ones with no or fixed solvent/electrolyte configura-

tions, to molecular dynamics approaches of both the full DFT (AIMD) and partially classical (QM/MM) varieties.

Explicit solvation approaches differ substantially both in computational cost and accuracy. Explicit AIMD of solvent and electrolyte (section 3.2) provides the most conceptually straightforward description of the electrochemical double layer, treating the entire system on an equal footing at the electronic structure level. However, using semi-local DFT for the explicit solvent has accuracy limitations for the electronic structure, underestimating the band gap due to self-interaction errors and leading to incorrect predictions of redox potentials [85] and interfacial band alignment [86]. Hybrid functionals with exact exchange or higher-level methods including GW many-body perturbation [87, 88] may capture solvent electronic structure more accurately, but at significant computational expense.

Replacing explicit DFT solvent with classical force field models in QM/MM methods (section 3.3) substantially reduces computational costs compared to AIMD, but these methods are limited by the accuracy of the solvent force field models and their interaction with the DFT. Overall, molecular dynamics approaches remain computationally expensive regardless of DFT or classical solvent. Most applications of first-principles methods to electrochemistry, especially for modeling electrochemical reactions, typically avoid dynamics entirely by omitting solvent and electrolyte, or using frozen configurations (section 3.1).

3.1. Fixed / no solvent

The simplest and currently most prevalent scheme of applying *ab initio* methods to address electrochemical challenges is the Computational Hydrogen Electrode (CHE) [25]. In its simplest form, this approach does not include electrification or solvation effects (section 1.4), predicting reaction potentials from neutral, unsolvated surface calculations alone using a linear free energy approximation (section 1.2). Here, we discuss approaches based on CHE that include varying levels of solvation and electrification.

The simplest form of the Computational Hydrogen Electrode model [25] captures the thermodynamics driven by change in potential, and can capture trends in electrochemical reactions that are driven by surface chemistry. However, it neglects the contributions of electrolyte, kinetic barriers, and electric fields, and cannot correctly capture the potential of zero charge or the capacitance. In particular, this model misses the complex nonlinear variation of grand free energy with potential for each configuration, because it implicitly linearizes the grand free energy about the neutral state as discussed in section 1.2.

The lack of solvation can be partially remedied by including a layer of explicit (DFT) solvent in the calculation. This is sufficient for certain applications, especially those that require identifying trends in reactivity. For example, a CHE approach with explicit water applied to water splitting reactions at metal surfaces elucidated the linear relationship between the binding strength of the adsorbates O, OH, and OOH with the surface. [89].

The CHE method may also be extended to describe the electrolyte, through addition of explicit, frozen (fixed, optimized geometry) electrolyte ions. Electrolyte ions are known to alter the properties of electrochemical systems. For instance, cations have been shown experimentally to significantly impact rates of the oxygen reduction reaction [90], the peak position of the hydrogen underpotential deposition on Pt [91], and the Stark tuning of CO on Pt [92]. Including explicit electrolyte also comes with the challenges discussed above: enhanced DFT self-interaction errors due to localized charges on ions, and the need for dynamics (section 2.2). It additionally introduces new challenges due to low ion concentrations which require large DFT supercells.

Frozen solvent may also be combined with any of the electrification schemes described in section 2.1. For example, Ref. [33] compares variants of the frozen solvent approach coupled with CHE, a constant field, and a uniform background charge to compute the reduction and oxidation of water on Pt(111). These electrification schemes differ in complexity and provide similar results for the simple configurations considered, but the choice of electrification method may matter for more complex adsorbate geometries, especially those with large dipoles [33].

The reduced computational cost of frozen solvent/electrolyte (extended CHE) techniques allows for a more extensive exploration of reaction mechanisms and electronic structure methods. However, the CHE strategy is intrinsically limited by the fact that fixed solvent configurations do not capture the thermodynamics or structure of liquid water at the interface [93]. Attempts have been made to capture the fluid thermodynamics using a continuum model, and chemical bonding and electronic structure effects from frozen configurations of a few explicit molecules. Such approaches require particular care because they can re-introduce the dynamics and accuracy issues of explicit and implicit electrolytes respectively. Additionally, in practice there is some amount of arbitrary decision-making in placing these solvent molecules. These limitations can be more fully addressed by moving from using fixed solvent structures to performing molecular dynamics, at additional computational expense and increased complexity of the simulation, as discussed next.

3.2. Ab initio molecular dynamics (AIMD)

Ab initio molecular dynamics (AIMD) treats the entire electrochemical interface in an electronic structure method such as DFT and samples the thermodynamic phase space of solvent configurations using molecular dynamics. This makes AIMD potentially the most accurate technique for first-principles electrochemistry in principle, but is limited by the substantially higher computational cost in practice. AIMD calculations must address many of the same challenges discussed above, including referencing the potential to an experimentally-measurable quantity and treat-

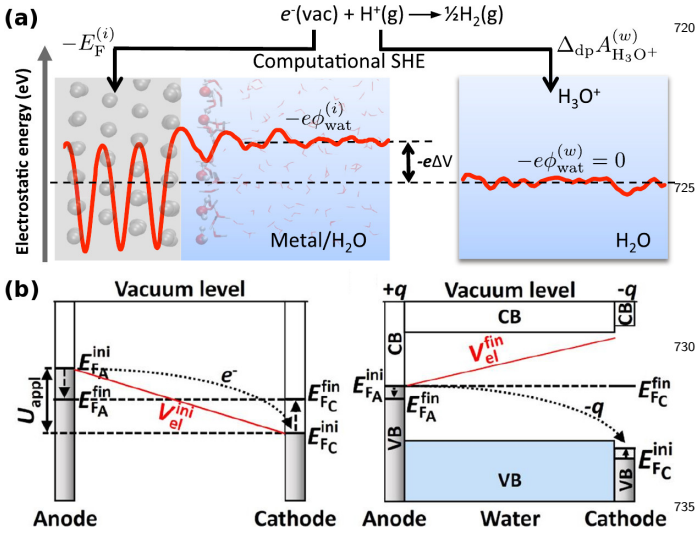

Figure 6: (a) Computational standard hydrogen electrode in *ab initio* molecular dynamics (AIMD) simulations by aligning electrostatic potentials in metal/water interface and bulk water simulations containing an excess proton [55]. (b) An electron reservoir approach in AIMD utilizing neon atoms as a wide-band gap counter-electrode to control charge and field in the remainder of AIMD unit cell [79]. (Adapted with permissions from Refs. 55 and 79.)

ing both the electrons and the electrolyte within the grand canonical ensemble appropriate for the thermodynamics of the electrochemical interface. While AIMD is still not yet computationally tractable for many electrochemical reactions, significant progress has been towards addressing these computational challenges.

The electron potential must be referenced to an experimentally accessible quantity. Early calculations referenced the electron potential to the water-vacuum interface [26], but large differences between the reference potentials and the potential range of interest introduce large errors. Using the solvation free energy of a proton in solution as an internal reference [45, 75] (Fig. 6(a)) leads to more accurate results. An extension of this hydrogen insertion method, or computational *standard* hydrogen electrode approach (distinct from the computational hydrogen electrode approach), has been successful for calculating the PZC of metal surfaces with AIMD [55].

As discussed in Sections 1.2 and 2.2, the grand canonical ensemble is the most convenient ensemble for computational electrochemistry. AIMD calculations have traditionally been designed in the canonical and microcanonical ensembles, in part because of the simplicity of these ensembles. These ensembles preserve the number of particles, whereas the grand canonical ensemble fixes the chemical potential of each species, a more difficult constraint to simulate. AIMD calculations in the grand canonical ensemble require a reservoir for excess particles, both electrons and ions, and the definitions of these reservoirs is an active area of research. While all ensembles are equivalent in the thermodynamic limit, the system-size convergence of molecular dynamics and Monte Carlo simulations can differ dramatically, with best convergence typically obtained in the grand canonical ensemble [94].

Current approaches to electron reservoirs include modifications of the electrostatic boundary condition deep within the liquid [78] and counter-ions with variable charge [79], analogous to the counter-sheet and ion electrification schemes shown in Fig. 5. Counter-ions that can serve as electron reservoirs must have a wide band gap, such as the modified neon atoms in Ref. [79], to allow varying the Fermi level (applied potential) over a wide range (Fig. 6(b)). Making simulations grand canonical in atoms or ions is much more challenging [79], and typically requires grand-canonical Monte Carlo (GCMC) techniques. Such techniques have typically been practical only for classical force-field simulations [95–97] due to the substantial computational cost of DFT calculations with Monte Carlo moves that substantially change geometries (and hence, the electronic structure) at each step. Although computationally inefficient, an alternative is to combine several canonical AIMD simulations with varying numbers of charge pairs with Monte Carlo sampling as a post-processing step [98].

Recent developments in AIMD simulations have made it possible to more accurately reference electrochemical predictions to the experimental scale and electrify the DFT unit cell. However, the computational cost of AIMD limits the number of solvent molecules and typically precludes the inclusion of electrolyte species in the calculation, as discussed in Section 2.2. Including a single counter-ion may approximate electrification, but does not correctly capture the long-range electrostatic potential and capacitance of the electrochemical interface. Additionally, semi-local DFT errors limit the accuracy of solvent structure in AIMD [99, 100], requiring more expensive methods such as hybrid functionals to improve accuracy. Alternate strategies to retain solvent and electrolyte dynamics while mitigating the computational limitations of AIMD are necessary to more broadly explore electrochemical phenomena in first-principles calculations.

3.3. Quantum mechanics / molecular mechanics (QM/MM)

QM/MM is a broad class of hybrid molecular dynamics techniques that treat a part of the system quantum mechanically, while approximating the remainder using classical force fields [101]. QM/MM has been widely applied in biochemistry and biology, particularly for protein studies, and sparingly for electrochemical applications [102, 103]. The promise of QM/MM is to retain the chemical accuracy of *ab initio* molecular dynamics at a much lower computational cost due to the reduced size of the quantum component of the simulation. This allows for longer simulation times and larger numbers of simulated atoms, which is important for accurate sampling of electrolytes, as discussed in section 2.2.

Realizing the full potential of QM/MM requires further developments on two fronts: accurate force fields for the classical region and reliable approximations for the interface between the classical and quantum regions. These

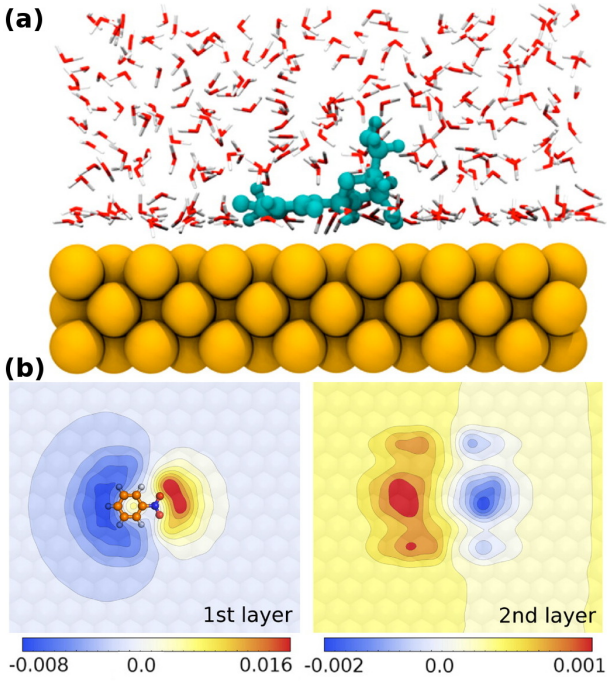

Figure 7: (a) Quantum mechanics/molecular mechanics approaches may partition electrode, electrolyte and surface species in numerous ways, *e.g.,* using different molecular mechanics approaches for the metal electrode and the electrolyte, surrounding a quantum molecule [104]. (b) Molecular mechanics models may treat metal electrodes using image charges, shown above for the top two atomic layers of Au(111) [105]. (Adapted with permissions from Refs. 104 and 105.)

requirements further depend on how the overall system is partitioned into classical and quantum regions. For example, in Figure 7(a), treating the metal surface and adsorbate in quantum mechanics surrounded by a classical liquid requires accurate force fields for the liquids alone. On the other hand, including the metal in the classical subsystem provides further opportunity for reducing computational costs, but requires treatment of metal polarization in a classical force field [104].

We first discuss the considerations in selecting force fields for the classical subsystem. Classical force fields vary in complexity from pair potentials with fixed charges; to polarizable and charge-equilibration force fields with variable local dipoles or charges; and to reactive force fields with dynamic bond connectivity. Increasing complexity in the force fields allows more accurate description of charge distributions in the classical subsystem, but introduces challenges in force field parameterization, especially when dealing with many atomic species. For example, classical molecular dynamics simulations of liquid water range from pair potential models such as SPC/E [106] and TIP4P [107, 108], through polarizable force fields [109], to charge-equilibration force fields [110–113]. The latter force fields provide an accurate description of the structure and dielectric response of liquid water, including at extreme temperatures, pressures and electric fields, but are specific to pure water. In contrast, pair potential models do not simultaneously capture thermodynamic and dielectric properties of water accurately [114], but parameterization of electrolytes in pair-potential models of water is relatively straightforward [115].

Classical force fields can either focus on specific material systems with highly detailed parameterization and potentially high accuracy for those materials as outlined above, or span large classes of materials, trading off accuracy. General-purpose force fields such as COMPASS [116], CHARMM [117] and AMBER [118] are intended for organic and biomaterials, while universal force fields (UFF) [119] address the entire periodic table with lower fidelity. On the other end of the spectrum, reactive force fields such as AIREBO [120], COMB [121] and ReaxFF [122] can potentially describe liquids and electrolytes in much more detail beyond the long-range charge response alone, including their chemical reactions. Most reactive force fields include a charge equilibration scheme based on electron affinities of each atomic species to capture variable charge states. In electrochemical simulations, this provides an additional opportunity to account for the fixed chemical potentials of the electrons within the liquid / electrolyte region in the vicinity of the electrode as well [123]. These reactive force fields require careful parameterization with extensive first-principles calculations for calibration, and their reliability is typically limited to a few atomic species and molecular environments. Thus, embedding in QM is generally still required to achieve the necessary chemical accuracy for the reactive portions of the simulation.

Machine learning may hold the key to addressing challenges in classical force-field parameterization by automatically generating them from DFT calculations [124, 125]. Further, using MM potentials developed using the same level of theory as in QM regions potentially increases the accuracy possible for QM/MM methods [126, 127]. At present, however, most machine-learned potentials (*e.g.,* gaussian-approximation potentials (GAP) methods [128]) only account for local interactions [129]; QM/MM for electrochemistry requires machine-learned potentials that also extract atomic charges [130] in order to correctly describe long-range interactions. Alternatively, physics-based empirical approaches such as density-functional tight-binding (DFTB) [131] models may provide another path forward for accurate QM/MM simulations of electrochemical systems.

In addition to accurate force fields for the classical region, QM/MM simulations also require reliable approximations for the interface between the classical and quantum regions. The QM/MM interface must both partition the atoms between classical and quantum regions, and describe the interactions between the two regions. The quantum region must include atoms in the vicinity of chemical processes of interest. Interfaces within liquids, in particular, require adaptive methods so that species can be either MM or QM depending on whether they have diffused in or out of a region in space designated as QM [101].

The accuracy of QM/MM depends on the treatment of electrostatic interactions across the interface. This can range from simple 'mechanical embedding' that describes the QM system with predetermined charges, through 'electrostatic embedding' that utilizes the QM charge density, to 'polarized embedding' that allows the MM charge to adjust self-consistently [101]. Complex interaction schemes incur greater computational expense, but can allow reduction in the size of the QM region for equivalent accuracy [132]. All these schemes exclude charge transfer across the quantum-classical interface, which limits the accuracy of electrostatic potentials in QM/MM [133].

Lastly, to further reduce computational cost, QM/MM calculations may include both the electrode and the electrolyte in the classical region [104]. However, classical treatment of metallic regions is particularly challenging due to the strong effects of polarization and the delocalization of charge [134–136]. These effects are difficult to capture in conventional polarizable and charge-equilibration schemes for atom charges, but are more naturally captured in image-charge response models of metals [105] (Fig. 7(b)). Application of such methods to electrochemistry requires further developments, especially in the image-charge treatment of non-neutral metal surfaces [135].

4. Implicit / continuum solvation models

The highly complex interactions between the atoms and electrons in the electrode and the electrolyte impact the equilibrium distributions of orientations, positions, and polarization of the solvent molecules and electrolyte ions. As discussed above, explicit solvation methods attempt to directly include these molecules and/or ions in the calculation, and need to invoke molecular dynamics to sample their distributions.

On the other hand, implicit / continuum solvation models break this complex problem into two simpler problems: describing *where* the solvent molecules or electrolyte ions are, and then, given this distribution, capturing *how* the electrolyte species respond to the electrode (Figure 8). This section presents a unified overview of the wide range of continuum solvation models applied to electrochemistry, discussing the physics they capture, strategies and inputs for parameterization, and their resulting accuracy for describing electrochemical properties.

Most continuum models approximate the distribution of solvent molecules near an electrode with a cavity: no molecules or ions in the region occupied by the electrode, and a uniform distribution outside it. The interactions between the electrolyte species and the electrode include mean-field electrostatic interactions and beyond mean-field effects including dispersion interactions, local repulsion, etc. Among these, the mean-field electrostatic interactions have the longest range and consequently most strongly impact the distribution of charges, and thus the energetics, of the electrode. The capability of continuum solvation

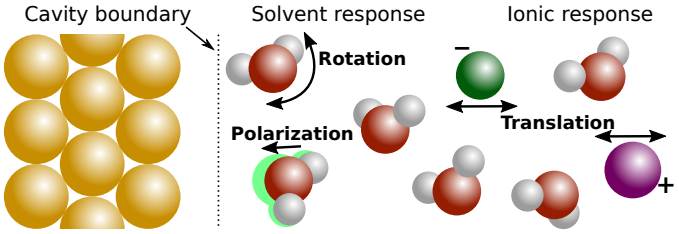

Figure 8: Continuum solvation models describe the equilibrium effect of electrolytes on electrodes by approximating the distribution of solvent molecules and ions near the electrode in the form of a cavity, and then approximating the interaction of the rotation, polarization and translation of molecules and ions with the electrode.

models to describe specific electrochemical phenomena depends most vitally on this interaction, which we describe in detail next in Section 4.1. All remaining interactions are described approximately in terms of the shape and size of the cavity, as we discuss in Section 4.3. The quantitative accuracy of both the dominant electrostatic interaction and the remaining secondary interactions depend on the precise size of the cavity and its proximity to the electrode. We discuss several approaches to determine and parameterize the cavity subsequently in Section 4.2.

4.1. Bulk response of electrolyte

The solvent and electrolyte interact with the electrode primarily through long-ranged electrostatic interactions between their charge densities. This interaction significantly contributes to interfacial properties such as capacitance and surface free energies. The net electrostatic potential that governs this electrostatic interaction is determined by Poisson's equation,

$$-\nabla^2\phi(\vec{r}) = \frac{\rho_{\text{tot}}(\vec{r})}{\epsilon_0}, \tag{1}$$

where the $\rho_{\text{tot}}(\vec{r})$ is the total charge density and ϵ_0 is the permittivity of free space.[9] The total charge density $\rho_{\text{tot}}(\vec{r}) = \rho_{\text{el}}(\vec{r}) + \rho_{\text{lq}}(\vec{r})$ includes the electrode charge density $\rho_{\text{el}}(\vec{r})$ in the electronic DFT calculation (electrons and nuclei) and the net charge density $\rho_{\text{lq}}(\vec{r})$ in the liquid region (solvent and electrolyte).

The net charge density in the liquid depends on the interactions of the liquid with the electrode, primarily through the dominant long-ranged electrostatic interaction mediated by the net electrostatic potential, $\phi(\vec{r})$. However, this "response" of the fluid is rather complicated in general with $\rho_{\text{lq}}(\vec{r}) = \rho_{\text{lq}}[\phi](\vec{r})$, a general functional where the charge density at one location $\vec{r}$ in space depends non-locally and non-linearly on the potential everywhere. Therefore, we can write the electrostatic potential in terms of the electrode charge density $\rho_{\text{el}}(\vec{r})$ from the electronic

[9] Note that many density-functional theory and continuum solvation model articles use atomic units with Gaussian/cgs system for electrical quantities, within which $\epsilon_0 = 1/(4\pi)$.

DFT calculation alone as

$$-\nabla^2\phi(\vec{r}) - \frac{\rho_{\rm lq}[\phi](\vec{r})}{\epsilon_0} = \frac{\rho_{\rm el}(\vec{r})}{\epsilon_0}, \tag{2}$$

but that is not feasible to solve directly in general.

To arrive at practical approximations to the fluid response, continuum models focus on the long-range potential alone, neglecting complexities in the short-ranged interactions at the atomic scale. Consequently, a multipole expansion is convenient to describe both the interaction of a charge distribution with an electrostatic potential and the potential generated by that charge distribution. The most important contributions will arise from the movement of net charges in the potential, which are monopoles at $l = 0$ in the multipole expansion. The next contribution will be from dipoles orienting to the gradient of the potential (the electric field), which is $l = 1$ in the multipole expansion. Subsequent terms involving quadrupoles at $l = 2$, octupoles at $l = 3$ and so on will become successively less important in the long-range limit.

The multipole components present depend on the nature of the species in the fluid. The monopole contribution requires net charges that can move independently in response to the electrostatic potential, which are only present in the electrolyte ions. Consequently, the $l = 0$ response dominates for electrolyte ions, and $l \geq 1$ contributions are less important. For neutral solvent molecules without a net charge, the monopole contribution is absent and therefore the $l = 1$ dipolar response dominates.

The picture so far is still fully general in terms of the locality of the response. This multipole expansion can, in principle, capture the effect of an atomic-scale charge distribution within the ion or molecule moving, rotating and polarizing in response to the electrostatic potential over the same length scales. Additionally making a linear-response approximation (with respect to electrostatic potential) allows the entire fluid response due to both molecules and ions to be written as a series of differential operators $\hat{D}^{(2l)}$ of order $2l$ for each multipole order,

$$\rho_{\rm lq}(\vec{r}) = \sum_{nl} w_{nl} * \hat{D}^{(2l)}\big(w_{nl} * \phi(\vec{r})\big) \tag{3}$$

along with convolutions $w_{nl}*$ to capture the nonlocality of the interaction, where n indexes different contributions at each l. This is the basis of the SaLSA continuum solvation model [18] that captures the nonlocal response of both solvents and electrolytes, but within a linear response approximation.

Most solvation models neglect this non-locality of the response, which effectively reduces all species in the fluid to point particles. In this limit, only the dominant multipole contributions of each species remains relevant, reducing the response to $l = 0$ alone for ions and $l = 1$ alone for solvent molecules. As we discuss next, this general perspective results in the family of Poisson-Boltzmann approaches.

The simplest model for the monopole response of ions is to treat them as an ideal non-interacting gas of particles, such that the local concentration of ions at any point is proportional to their potential energy. For a general electrolyte with several species of ions with charges Z_i and bulk concentrations N_i (satisfying $\sum_i N_i Z_i = 0$ for charge neutrality), this results in an ionic charge density

$$\rho_{\rm lq}^{\rm ion}(\vec{r}) = \sum_i N_i Z_i e \exp\left(\frac{-Z_i e\phi(\vec{r})}{k_B T}\right), \tag{4}$$

where e is the elementary charge. For a symmetric $Z:Z$ electrolyte containing cations and anions of charges $\pm Z$ with the same bulk concentration $N_{\rm ion}$, the above simplifies to

$$\rho_{\rm lq}^{\rm ion}(\vec{r}) = -2N_{\rm ion} Ze \sinh\left(\frac{Ze}{k_B T}\phi(\vec{r})\right). \tag{5}$$

At low potentials where $Ze|\phi| \ll k_B T$, we can approximate $\sinh(x) \approx x$ and substitute back into the Poisson equation to yield the linearized Poisson-Boltzmann equation

$$-\nabla^2\phi(\vec{r}) + \frac{\phi(\vec{r})}{\lambda^2} = \frac{\rho_{\rm el}(\vec{r})}{\epsilon_0}, \tag{6}$$

with the Debye screening length λ given by

$$\lambda^{-2} = \frac{2N_{\rm ion} Z^2 e^2}{\epsilon_0 k_B T}. \tag{7}$$

(Note that ϵ_0 will be replaced by ϵ_b, the net dielectric permittivity of the electrolyte after accounting for the solvent dielectric response below.) The solution to the linearized Poisson-Boltzmann equation in regions without charge takes the form $e^{-r/\lambda}$, causing the potential to exponentially decay with a characteristic length scale given by the Debye screening length λ.

More generally, without making the small potential approximation above, the Poisson-Boltzmann equation for a symmetric electrolyte is

$$-\nabla^2\phi(\vec{r}) + \frac{\phi(\vec{r})}{\lambda(\phi)^2} = \frac{\rho_{\rm el}(\vec{r})}{\epsilon_0}, \tag{8}$$

with a potential-dependent Debye screening length $\lambda(\phi)$ given by

$$\lambda^{-2}(\phi) = \frac{2N_{\rm ion} Ze}{\phi} \sinh\left(\frac{Ze}{k_B T}\phi\right). \tag{9}$$

Figure 9(a) compares the Debye screening length of aqueous 1:1 ($Z = 1$) electrolytes at $N_{\rm ion} = 1$ mol/liter in the linearized and nonlinear potential-dependent forms. As expected, the linear form is appropriate only when the potential satisfies $Ze|\phi| \ll k_B T$ (lower x-axis), which corresponds to $\phi \ll 0.026$ V at room temperature of 300 K (upper x-axis). The Debye length exponentially decays to zero with increasing potential, which corresponds to an ionic charge density $\rho_{\rm lq}^{\rm ion} \propto \lambda^{-2}$ that diverges to infinity.

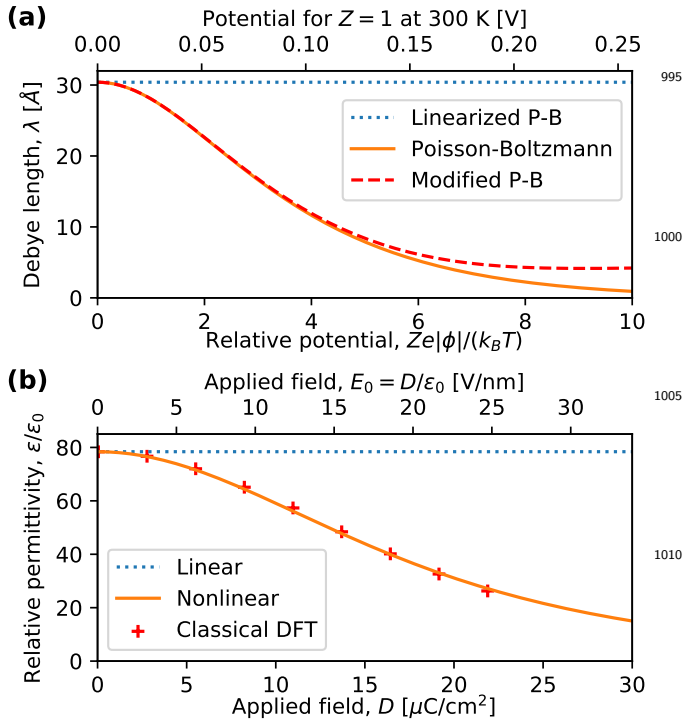

Figure 9: (a) Nonlinear Debye screening length due to Poisson-Boltzmann ionic response, and its saturation (lower bound) due to ion packing in the modified Poisson-Boltzmann (mPB) approach [137], shown for 0.01 M aqueous KPF_6 (assuming 2.4 Å and 2.8 Å ionic radii). (b) Nonlinear dielectric response of water due to saturation of dipole rotations, captured in the NonlinearPCM solvation model [13] and classical DFT [114, 138].

This is an unphysical consequence of assuming that the ions are non-interacting. The modified Poisson-Boltzmann approach [137] mitigates this issue by enforcing a 'packing limit' on the ions, resulting in

$$\lambda^{-2}(\phi) = \frac{2N_{\text{ion}}Ze}{\phi}\frac{\sinh\left(\frac{Ze}{k_BT}\phi\right)}{1+2\eta\left(\cosh\left(\frac{Ze}{k_BT}\phi\right)-1\right)}, \qquad (10)$$

where $\eta = N_{\text{ion}}\sum_i(4\pi R_i^3/3)$ is the volume fraction of ions with radii R_i (i = cation, anion) in the bulk electrolyte. Figure 9(a) shows that this modified Poisson-Boltzmann equation results in a lower bound on the Debye screening length, corresponding to an upper bound in the concentration and charge density of the ions. Without this upper bound, the Poisson-Boltzmann equation may lead to an unphysical pile-up of ionic densities near the electrode and a corresponding divergence of the solvation energetics [13].

As discussed above, the monopole $l = 0$ response dominates for ions in the local response limit, while for neutral species like solvent molecules, the monopole response is forbidden and the dipole $l = 1$ response dominates. Unlike the monopole response corresponding to translational motion of charges, there are two classes of response that contribute at the dipole order. First, analogous to the movement of charge monopoles, molecules with permanent dipoles can rotate to align with the electric field, creating a net dipole moment with contributes an induced charge density. Additionally, the electric field can polarize the molecules both by distorting the electron density and by stretching / bending bonds, creating an *induced* dipole which contributes an induced charge density. In both cases, each molecule in the fluid generates a net dipole moment $\vec{p} = C\alpha\vec{E}$ in response to the local electric field $\vec{E} = -\nabla\phi$, where α is the polarizability of the molecule. The local field coefficient, C, is a constant that accounts for the difference between the local electric field seen by the molecule, compared to the net electric field $\vec{E}$ which includes the contribution of that molecule and its surroundings. Mean-field theory with $C = 1$ is inadequate except for extremely dilute gases. For liquids with low dielectric constants, determining C by placing the molecule in a spherical cavity of the net dielectric constant determined self-consistently (*i.e.*, Clausius-Mossoti theory [139]) works much better. High dielectric constant, polar liquids like water typically require more advanced theories of the correlated response of molecules [140], or an empirical approach as we will discuss below.

In a solvent with density N_{lq} of the molecules described above, the electric field induces a polarization density $\vec{P} = N_{\text{lq}}\vec{p}$, which in turn leads to an induced charge density of the solvent

$$\rho_{\text{lq}}^{\text{solv}}(\vec{r}) = -\nabla\cdot\vec{P} = \nabla\cdot(N_{\text{lq}}C\alpha\nabla\phi(\vec{r})). \qquad (11)$$

For a uniform fluid without any ions, substituting back into the Poisson equation, reduces it to the form

$$-\nabla^2\phi(\vec{r}) - \nabla\cdot\left(\frac{N_{\text{lq}}C\alpha}{\epsilon_0}\nabla\phi(\vec{r})\right) = \frac{\rho_{\text{el}}(\vec{r})}{\epsilon_0}, \qquad (12)$$

which can be rearranged to $-\nabla^2\phi = \rho_{\text{el}}/\epsilon_b$ with an effective bulk dielectric constant

$$\epsilon_b = \epsilon_0 + N_{\text{lq}}C\alpha. \qquad (13)$$

Each of the contributions to the overall dipole response including polarization and rotation contribute a term above with a separate polarizability α.

The electronic and vibrational polarizability of the molecule contribute an α_{pol} that is typically assumed constant with respect to field strength E. This is because the characteristic energy and length scales of this response are several eV and a few Å respectively, requiring fields substantially exceeding the V/Å $= 10^{10}$ V/m scale in order to modify the response substantially. However, the rotational response of permanent molecular dipoles, such as in liquid water, occur at the much smaller thermal energy scale $\sim k_BT$ (0.026 eV at room temperature). Correspondingly, this response may be strongly affected by fields on the 10^8 V/m scale, which is easily exceeded at an electrochemical interface. In particular, a typical electrode surface charge density of 10 μC/cm^2 corresponds to an electric field of 1.1×10^{10} V/m or 11 V/nm, and fields of this magnitude

have been measured experimentally using the vibrational Stark effect in a number of material systems [141, 142]. It is therefore vitally important to account for the nonlinear rotational response of solvents.

The simplest model for the rotational response of solvent molecule dipoles, much like the corresponding case for ions above, assumes the dipoles all respond freely and independently to the external field. A simple statistical-mechanical derivation writing out the Boltzmann probabilities for dipoles aligning to the field with potential energy $-\vec{p}\cdot C_{\text{rot}}\vec{E}$ [139] and computing the average dipole moment yields the field-dependent polarizability

$$\alpha_{\text{rot}}(E) = \frac{p_{\text{mol}} C_{\text{rot}}}{E} \coth\left(\frac{p_{\text{mol}} C_{\text{rot}} E}{k_B T}\right) - \frac{k_B T}{E^2}. \quad (14)$$

Here p_{mol} is the magnitude of the solvent molecule dipole and C_{rot} is the rotational contribution to the local field coefficient discussed above. This polarizability has the highest value of $(p_{\text{mol}} C_{\text{rot}})^2/(3k_B T)$ for low electric fields $E \to 0$. It reduces in magnitude with increasing E when most dipoles have aligned completely with the field, resulting in saturation of the response. The net dielectric constant of the fluid is therefore

$$\epsilon_b(E) = \epsilon_0 + N_{\text{lq}}(C_{\text{pol}}\alpha_{\text{pol}} + \alpha_{\text{rot}}(E)). \quad (15)$$

The local field coefficients C_{pol} and C_{rot} for the polarization and rotational responses can be determined by matching the $E \to 0$ limit of the dielectric response to experiment. Specifically, matching $\epsilon_b(E)$ to the low-frequency dielectric constant ϵ_b (≈ 78.4 for water at 300 K), and matching ϵ_b without the rotational term to the experimental optical-frequency dielectric constant ϵ_∞ (≈ 1.8 for water) yields two conditions that fix both C_{pol} and C_{rot} [13, 114].

Figure 9(b) demonstrates for water that $\epsilon_b(E)$ varies significantly with applied field, and that $\epsilon_b(0)$ only approximates $\epsilon_b(E)$ at the smallest applied field strengths. The simple model described above, incorporated into the NonlinearPCM solvation model [13], agrees very well with a more detailed classical density-functional theory prediction for the nonlinear dielectric response [114]. Specifically, note that the relative permittivity of water reduces by a factor of two for a surface charge density of 15 μC/cm^2, a rather nominal value for electrochemical interfaces. It is therefore critical to include nonlinear dielectric response in solvation models used for first-principles electrochemistry. Most continuum solvation models in widespread use currently do not include it as detailed in section 4.4, which lead to an incorrect qualitative description of electrochemical capacitance as discussed in section 4.5.

Above, we have discussed models for the nonlinear response of electrolyte ions and solvent molecules in a bulk fluid. For a continuum solvation model, the fluid will only be present in the region not occupied by the electrode or any adsorbates or surface species treated using electronic DFT. As discussed next in section 4.2, this is described by a cavity shape function $s(\vec{r})$ that is zero in the electrode region and one in the bulk fluid region. With that modification, the electrostatic potential $\phi(\vec{r})$ in a local-response continuum solvation model is very generally given by the generalized Poisson-Boltzmann equation

$$-\epsilon_0\nabla^2\phi(\vec{r}) - (\epsilon_b(|\nabla\phi|) - \epsilon_0)\nabla\cdot(s(\vec{r})\nabla\phi(\vec{r})) + \frac{\epsilon_b s(\vec{r})\phi(\vec{r})}{\lambda(\phi)^2} = \rho_{\text{el}}(\vec{r}). \quad (16)$$

This is obtained from the above by modulating the bulk solvent density N_{lq} and ion density N_{ion} by the cavity shape function. Different local solvation models assume different simplified models for $\epsilon_b(E)$ and $\lambda(\phi)$, with the simplest limit being the fully linearized Poisson-Boltzmann where $\epsilon_b(E)$ and $\lambda(\phi)$ are each replaced by their low-field and low-potential limits.

4.2. Defining the cavity

The previous section discusses *how* the solvent and electrolyte environment respond; a complete model for the electrochemical interface must also account for *where* this environment response is present. Continuum solvation models approximate the real atomic-scale environment response with the bulk environment response *outside* the solute (electrode) region modeled explicitly in the first principles calculation. All these models effectively scale the bulk response by a cavity shape function $s(\vec{r})$ that switches from zero in the solute region to one in the solvent region, but differ substantially in how they parameterize and determine $s(\vec{r})$. Additionally, for an electrolyte, a shape function $s_{\text{ion}}(\vec{r})$ determines where the ions respond, which in general could be different from $s(\vec{r})$. We first discuss the solvent cavity $s(\vec{r})$ in detail below, before discussing similar considerations for the electrolyte cavity at the end of this section.

Intuitively, the solvent cavity shape function $s(\vec{r})$ accounts for the fact that solvent molecules can reach the solute or electrode surface up to a distance of nearest approach, which limits the spatial extent of their response. However, the spatial extent of the response is not precisely defined by the location of the solvent molecules, either in terms of their geometric centers or their constituent atoms (Figure 10(a-b)). The primary reason for this difference is that, fundamentally, the response is *nonlocal* at the atomic scale. For example, the rotation of a water molecule dipole depends on the electric field over the spatial extent of the molecule, and produces a charge distribution over this spatial extent as well.

Most continuum solvation models approximate the response as *local*, and in order to reproduce the energetics of the true non-local response, they should still produce induced charge density at the correct locations (Figure 10(c)). This implies that the effective local response must extend closer to the solute than the location of the geometric centers of molecules. Consequently, the cavity needs to 'switch on' somewhere between the distance of

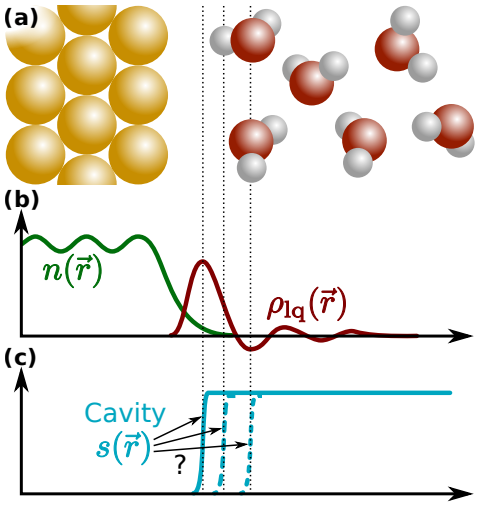

Figure 10: (a) Schematic distance of nearest approach of atoms in solvent molecules near an electrode surface, compared to (b) the electron density $n(\vec{r})$ of the electrode and induced charge density $\rho_{\mathrm{lq}}(\vec{r})$ in the solvent. (c) Local solvation models require cavity shape functions $s(\vec{r})$ that transition at the induced charge density peak, rather than solvent atom approach distances.

nearest approach of solvent geometrical centers (farther from solute) and that of the solvent atomic or electronic charge densities (nearer to solute). In most cases, this cavity distance requires empirical parameterization. Solvation models with nonlocal response [18] can mitigate this empiricism, as described below in Section 4.4, but most continuum solvation models employ local response because of easier implementation and lower computational cost.

Despite the complexities discussed above, ultimately, the cavity correlates with the distance of nearest approach of solvent molecules to the solute. This distance is related to the effective sizes of the constituent atoms for nonbonded interactions, often described using van der Waals (vdW) radii. The atom size, in turn, arises from the strong repulsion when electron densities of two atoms overlap. Therefore, continuum solvation models have adopted two broad classes of strategies to determine the cavity $s(\vec{r})$: atomic spheres based on empirical atomic radii, and iso-density approaches based on electron densities.

Atomic sphere cavities use atomic radii to define the solute region ($s = 0$) based on a union of spheres centered on the atoms of the solute. The simplest approach directly defines the cavity as a union of atom-centered spheres, with radii that account for the solute atom radius and an additional empirical distance to the start of the solvent response. More complex approaches first estimate the cavity governing the solvent molecule centers, called the solvent accessible surface (SAS), from atom-centered spheres with radii equal to the sum of solute atom and solvent molecule radii. They then remove spheres of an empirical radius centered on the SAS to form a smaller cavity ($s = 0$ region), called the solvent excluded surface (SES), which then determines the location of the response (Fig. 11). This approach results in a smoother cavity surface and avoids spurious placement of solvent response in small gaps between solute atoms. See Ref. [143] and [144] for comprehensive reviews on the large number of approaches used for atomic-sphere cavity determination in traditional solvation methods.

On the other hand, iso-density approaches correlate the position of the cavity to the electron density of the solute. They typically allow the solvent response ($s = 1$ region) to occupy all space where the solute electron density $n(\vec{r})$ is smaller than a characteristic value n_c, below which it is assumed to not significantly repel the solvent. In this case, n_c is treated as an empirical parameter that controls the size of the cavity that directly determines the location of the solvent response (Fig. 11).

Comparing the two types of approaches, atomic-sphere based parameterizations are highly flexible, with potentially a large number of parameters that can be adjusted to deliver high accuracy in domains with a lot of data to parameterize the models. They are predominant in describing the solvation of organic molecules, for which extensive solvation free energy databases from thermochemical measurements can be used for fitting a large number of atomic radii and scale parameters. On the other hand, iso-density cavity approaches typically incur fewer parameters, such as a single global n_c for a solvent, making them more transferable to domains with less reliable data.

Both the atomic radius and the electron density approaches define a surface at which the solvent cavity turns on. The solvent-solute transition can either occur abruptly in space across this surface, or smoothly over some distance. This smoothing function can serve two purposes: to approximate the nonlocal nature of this transition, and to improve the numerical stability of *ab initio* calculations near these interfaces. Smooth solvation cavities are particularly important for the stability of *ab initio* calculations employing a plane-wave basis sets and those performing molecular dynamics [11, 145, 146]. Implementations vary in the precise functional form for deriving $s(\vec{r})$ from $n(\vec{r})$, including a function of $\log(n/n_c)$ transitioning over a width σ [13, 70, 147] or a sigmoidal function transitioning over a range n_{min} to n_{max} [11, 12], but generate very similar results when parameterized to the same data sets [148].

These cavity definition strategies, originally developed for the solvation of small organic molecules [143], are particularly successful when the charge density is comparatively uniform and unchanging for the same atomic species in different chemical environments. However, these approaches have been less successful for charged species and electrochemical interfaces. Charged species are problematic for the atomic radius strategy because species with different charges, and hence different electron densities at the surface, are treated using the same atomic radii. The electron density approach does not resolve this problem either because positive and negative charges affect the solvent in different ways with different magnitudes, and this effect is not captured by a simple electron density thresh-

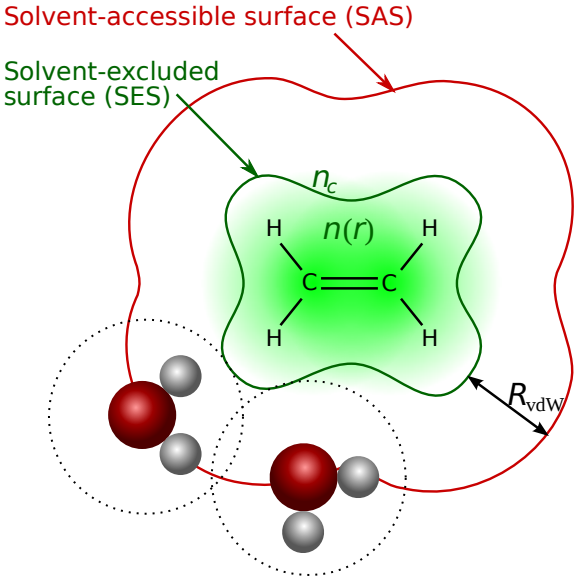

Figure 11: Atomic-sphere cavities typically define an outer solvent-accessible surface (SAS), from which an inner solvent-excluded surface (SES) defining the location of the solvent response is constructed. Iso-density approaches define cavities by thresholding the electron density $n(\vec{r})$ and typically correspond directly to the solvent-response surface (SES). (Adapted with permission from Ref. 150.)

old. This effect is solvent specific. For instance, water more strongly solvates anionic species relative to cations and neutral molecules, effectively requiring a smaller cavity for anionic species to account for this effect [149]. Acetonitrile has the opposite response, more strongly solvating cationic species [17]. Intuitively, this charge asymmetry occurs because of the asymmetry in the solute accessibility of the solvent. In the case of water, the positive charge center (the hydrogen) can more closely approach the solute, favoring solvation of negatively charged species. For acetonitrile, the negative charge center (the nitrogen) is more solute-accessible than the buried but positively charged central carbon atom.

Continuum solvation models do not automatically capture such charge asymmetry effects because they reduce molecules to point dipoles. Some solvation models empirically address the charge asymmetry problem by defining separate parameters for anionic and cationic cavities [149]. This reduces solvation energy errors, but application of these solvation models is limited to systems with only one charged species, excluding the study of systems such as zwitterions and ionic surfaces. A more general approach is a cavity that dynamically contracts or expands in response to the local electric field, capturing the asymmetry of solvation within a single parameterization [17, 151].

The approaches described above for handling charged species are all intrinsically empirical, requiring fitting parameters and/or a choice of functional form in the dependence of cavity size on local electric field [17, 149, 151]. Extensive databases of molecular solvation free energies are available to determine these fitting parameters and functional forms for solvation models for organic species and small ions [152–154]. Describing solvation at electrochemical (charged) interfaces is challenging for similar reasons as charged ions and molecules. However, interfaces are additionally difficult to benchmark because similarly systematic experimental data sets for calibrating interfacial solvation do not yet exist. Most continuum solvation studies of electrochemical interfaces so far employ models parameterized exclusively to molecular and ionic data sets. Improving the accuracy and reliability of electrochemical solvation requires alternate strategies to define cavities at charged interfaces and to benchmark energetics of charged surfaces.

The above discussion focuses on the cavity $s(\vec{r})$ that defines the dielectric response of the solvent. Describing an electrolyte requires an additional cavity $s_{\text{ion}}(\vec{r})$ that defines the ionic response of the electrolyte, which should be distinct from $s(\vec{r})$ in general. In fact, the concept of an "ionic cavity" predates solvation models and is implicit in the Gouy-Chapman-Stern (GCS) model of the electrochemical double layer [34]. Electrolyte ions are limited in their approach to the surface because of their solvation shells, leaving a region adjacent to the electrode with solvent alone (Fig. 2(a)). The width of this solvent-only region, typically denoted x_2, is therefore approximately equal to the solvated radius of the electrolyte ions. (This notation follows from defining x_1 as the width of the 'vacuum gap' between the electrode and the solvent-only region, as shown below in Fig. 12(a).)

Construction of a separate ionic cavity $s_{\text{ion}}(\vec{r})$ should be straightforward in principle based on the above considerations. However, a combination of numerical challenges and parameterization issues makes ionic cavities more difficult to define, and most prior solvation models applicable to electrochemical systems utilize a single cavity for both solvent and ionic response [12–14, 17, 18, 70, 149, 155]. Numerical challenges in defining ionic cavities result primarily from the greater distance of the ionic cavity from electrode atoms, larger by x_2 compared to the solvent cavity. Solvation models applied to electrochemistry predominantly employ iso-density cavity parameterizations, which will require an extremely low n_c to describe a further-away ionic cavity due to the exponential decay of electron density away from the surface. This exponential decay constant will additionally differ between electrodes depending on their work function and resulting orbital localization precluding a single, numerically-stable n_c that can capture a given x_2 for different electrodes. These numerical challenges may be avoided either by using an atomic parameterization with x_2 added to the atomic radii [65], or by using convolution tricks to expand iso-density solvent cavities by a specified width x_2 independent of the electron-density exponential decay constant [150].

The greater challenge in defining ionic cavities is identifying reliable experimental data to parameterize x_2. As discussed above, solvation cavity parameterization relies on extensive thermochemical databases of solvation free

energies determined from temperature-dependent solubility measurements [152]. Importantly, the solvation energies depend primarily on the solvent dielectric response even for solvation in electrolytes, especially with highly-polar solvents like water in aqueous electrolytes. The solvent region strongly screens the electric field of the electrode and thereby reduces the energetic contribution of electrode-ion interactions. Correspondingly, thermochemical data do not constrain x_2 sufficiently to identify deviations from the zeroth-order guess of x_2 = ion radius, such as reduction of x_2 with increasing field strength as ions are strongly attracted to the interface, or asymmetry with the field direction due to different ionic sizes. Precise parameterization of ionic cavities therefore require experimental measurements of ion distributions, which are significantly more challenging and sparsely available than solvation energies. Accurately capturing field-dependent ionic cavities may be important in future work for correctly predicting the electrostatic potential and capacitance in first-principles calculations of electrochemical interfaces.

4.3. Non-electrostatic free energy terms

Continuum solvation models adopt several approaches to define the cavity that separates the continuum liquid (or electrolyte) subsystem from the solute (or electrode) subsystem treated using DFT, and make different levels of approximations for the electrostatic interaction between these subsystems as discussed above in Sections 4.2 and 4.1 respectively. The electrostatic interaction is the dominant contribution to the overall effect of solvation on energetics, especially for highly charged systems, but accurate modeling of free energies in solvated environments requires accounting for the sub-dominant non-electrostatic interactions as well. Briefly, the three most important physical effects that contribute beyond the electrostatic interaction are the cavitation free energy required to remove liquid from a region of space and replace it with the solute, dispersion interactions between solute and solvent, and the repulsion between these subsystems [143]. Solvation models either treat these physical effects separately in detail, or adopt an empirical approach for their overall energetic contribution, as we discuss below.

The cavitation free energy, defined as the free energy cost of forming the cavity in the solvent, exhibits a complex dependence on the size and shape of atomic-scale cavities relevant for solvation as predicted by molecular dynamics simulations [114, 156]. It reduces to the surface tension energy proportional to the cavity surface area in the macroscopic limit of large cavities, but transitions to a volume-proportional contribution over cavity dimensions comparable to the solvent-molecule size. Solvation models can estimate size-dependent cavitation free energies using scaled-particle theory estimates for spherical cavities [157–159]. More generally, nonlocal models based on convolutions of $s(\vec{r})$ derived from classical density-functional theory can efficiently describe the cavity size and shape dependence of this free energy contribution [150]. It is important to account for this dependence because the net cavitation free energy for atomic-sized cavities is significantly smaller than the estimate based on macroscopic surface tension and the cavity surface area.

While cavitation results from a modification of the solvent distribution, the remaining effects are a consequence of solvent-solute interactions. Dispersion interactions are longer-ranged attractive interactions with an r^{-6} dependence on separation, and proportional to the atomic polarizabilities of the interacting species [160, 161]. Repulsion interactions resulting from solute-solvent electron overlaps are shorter-ranged with an exponential decay with separation [143]. The finite range of these interactions makes their energy contributions dependent on the size and shape of the cavity; this dependence is approximately proportional to the surface area only for cavities much larger than the range of interaction. Nonlocal dispersion models [150] that directly employ pairwise interactions between solute and solvent atoms [160, 161] capture the size and shape dependence automatically. These approaches often also combine repulsion and dispersion into a single 'interaction contribution' to the non-electrostatic free energy [162].

Several solvation models instead employ an overall empirical approach to the non-electrostatic contribution, such as $E = \alpha S + \beta V$, combining terms proportional to the surface area S and volume V of the cavity, scaled by fitting parameters α and β [12, 13]. Importantly, the coefficient α is an empirical effective tension that differs from the surface tension of the liquid because of the size and shape dependence of cavitation discussed above, and because it also includes dispersion and repulsion contributions. The volume term βV can improve fits to solvation energies of molecules [12], but is not meaningful for surface slab calculations used for electrochemical interfaces since the cavity volume then depends on the number of layers and diverges in the macroscopic limit. Therefore, electrochemical calculations should exclusively use non-electrostatic parameterizations with surface terms alone, or the more detailed nonlocal models discussed above.

Additionally, an empirical effective tension α depends only on the solvent and does not account for the solute dependence of the repulsion and dispersion terms contained within. For example, such models for water with a positive α for water [12–14] predict a positive interfacial energy for metal-water interfaces [163], while models with explicit dispersion terms [17, 18] result in a net-negative interfacial energy because the attractive dispersion contribution exceeds cavitation and repulsion in this geometry. Some atomic-cavity solvation models [164] address this with solute-atom-dependent cavity tension parameters, but this results in a large number of parameters that makes parameterization significantly more challenging.

Finally, empirical models of the non-electrostatic term introduce fitting parameters such as α and β that may be highly covariant with the parameters that determine cavity size (such as n_c or $\{n_{\min}, n_{\max}\}$), making the reliable determination of these parameters from solvation

Model	Response		Cavities		Year
	ϵ	κ	Type	$x_2 \neq 0$	
Linear response					
Gygi et al. [145]	L	none	n	No	2002
SCCS [12, 149]	L	L	n	No	2012
LinearPCM [13, 70] = VASPsol [14]	L	L	n	No	2013 2014
CANDLE [17]	L	L	$\bar{n}, \phi$	No	2015
SaLSA [18]	L	L	$\bar{n}$	No	2015
Soft-sphere [155]	L	none	Atom	No	2017
Nonlinear response					
DFT+mPB [166]	L	NL	n	Yes	2008
Dabo et al. [167]	L	NL	n	Yes	2010
NonlinearPCM [13, 148]	NL	NL	n	No	2013
NESS [65]	NL	NL	Atom	Yes	2018

Table 1: Categorization of solvation models for electrochemistry by linearity of fluid dielectric (ϵ) and ionic (κ) response, cavity parameterization type, and presence of a separate ionic cavity ($x_2 \neq 0$). Here L = linear, NL = nonlinear, n = solute electron density (iso-density models), ϕ = solute electrostatic potential and Atom = atomic spheres. $\bar{n}$ is nonlocal electron density. Modified with permission from Ref. [65].

energy databases more challenging [165]. At present, for the specific solvation models applicable to electrochemical systems discussed below (Table 1), only SaLSA [18] and CANDLE [17] employ nonlocal cavitation and dispersion models [150] that avoid empirical tension parameters. The choice of non-electrostatic free energy model impacts energy calculations necessary for reaction energy predictions, but does not affect the electrostatic potential that determines charging behavior and capacitance of electrochemical interfaces. We focus on electrostatic potential variations in the remainder of this review and therefore do not discuss non-electrostatic energy terms in the comparisons between models below.

4.4. Solvation model implementations

The previous sections outline the three main components of continuum solvation models: electrostatic response, fluid distribution (cavity determination) and non-electrostatic energy contributions. In addition, implementations of solvation models differ greatly between finite basis set codes used for molecular simulation and plane-wave DFT codes used for surface calculations. Correspondingly, solvation models in finite basis set codes, including the SMx (Solvation Model x) series [164, 168, 169] and the PCM (Polarizable Continuum Model) series [143, 144, 170, 171], are parameterized and applied predominantly to organic molecules in solution. See Ref. 143 for a detailed review of these models.

Here, we focus on solvation models developed for plane-wave DFT that are suitable for first-principles calculation of electrochemical interfaces. Table 1 compares such solvation models based on their electrostatic response (Section 4.1) and cavity determination technique (Section 4.2) which strongly affect the predicted electrochemical capacitance and charge distributions, as we discuss below in Section 4.5. We ignore details in the non-electrostatic energy contributions (Section 4.3) which are important for reaction energy predictions, but do not affect capacitance.

The vast majority of solvation models employ a linear response approximation for both the dielectric (ϵ) and ionic screening (κ) of the fluid; this is also the case for most finite basis-set solvation models [143, 144, 164, 168–171] not shown in Table 1. Only a small subset of the solvation models in plane-wave DFT codes capture nonlinearity in the ionic or dielectric response [13, 65, 148, 166, 167].

Most solvation models employ a smoothened iso-density cavity [11, 145] parameterized either in terms of an electron density range $\{n_{\min}, n_{\max}\}$ as in the self-consistent continuum solvation (SCCS) models [12, 149], or a critical electron density n_c as in the joint density-functional theory (JDFT) based solvation models [13, 14, 70, 147]. Iso-density cavities may exhibit instabilities for surfaces of non-close-packed solids due to low electron density in voids that may get incorrectly filled with fluid [150]. Nonlocal cavities determined from the overlap of solute and solvent electron densities ($\bar{n}$) avoid such issues by ensuring that the fluid only occupies regions of space that can fit an entire solvent molecule [17, 18].

Finally, most solvation models currently used for first-principles electrochemistry use the same cavity for the dielectric and ionic response, effectively setting $x_2 = 0$. Only one model shown in Table 1 includes a separate ionic cavity ($x_2 \neq 0$), nonlinear dielectric response, and nonlinear ionic response, all of which are necessary to predict electrochemical capacitance correctly, as we discuss next.

4.5. Example: capacitance of Ag(100)

The ultimate goal of solvation models for electrochemistry is to accurately predict potential-dependent charge distributions and their impact on energetics and reaction mechanisms at the interface. Here, we delineate the importance of each solvation model component discussed above by comparing electrochemical capacitance predictions against measurements for a single-crystal Ag(100) electrode in an aqueous non-adsorbing electrolyte (Figure 12). The experimental capacitance (dashed black line in Figure 12(b)) is roughly symmetrical about the potential of zero charge indicated by the vertical line at the center of the plot. This system exhibits the 'double-hump' behavior of an ideal electrochemical interface with non-adsorbing electrolytes. The minimum at the potential of zero charge arises from the low ionic capacitance in the diffuse electrolyte region for the neutral interface, as shown schematically in Fig. 2(b).

We consider a model of the electrochemical interface, Figure 12(a), containing features of the interface that may be necessary for a correct description of the capacitance with potential. Specifically, we consider a vacuum-only region with width x_1, a solvent-only region with width x_2, dielectric nonlinearity $\epsilon(E)$ and ion-packing effects treated

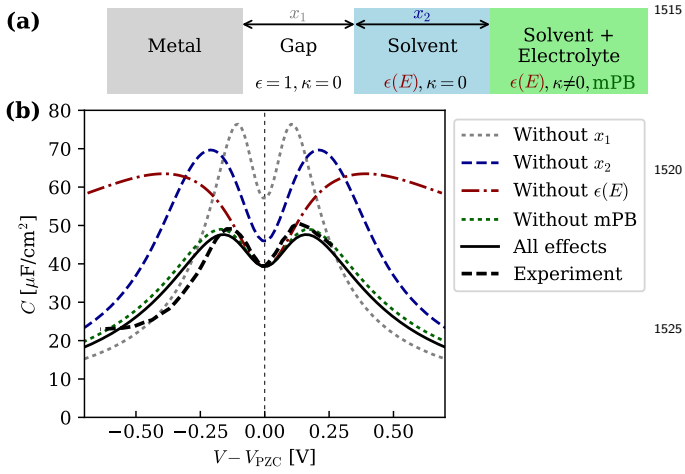

Figure 12: (a) Series capacitance model for a metal immersed in a non-interacting electrolyte with vacuum gap (x_1) and solvent-only (x_2) regions between electrode and electrolyte. (b) Capacitance predictions including x_1, x_2, nonlinear dielectric ($\epsilon(E)$) and modified Poisson-Boltzmann (mPB) agrees with experimental measurements of Ag(100) in aqueous 0.1 mol/L KPF_6 electrolyte from Ref. 172. Each of these features (except mPB) is critical to obtain a qualitatively correct variation of electrochemical capacitance with potential. (Adapted with permission from Ref. 65.)

using a modified Poisson-Boltzmann (mPB) approach. The model capacitance including all of these features (solid black line in Fig. 12(b)) is in good agreement with the experimental capacitance. The remaining lines in Fig. 12(b) depict the capacitance of the model with each one of these four features excluded. Except for mPB, all remaining features of this model are necessary for achieving quantitative agreement with experiment.[10]

The first two features control the spatial structure (*i.e.*, solvation cavities) of the model, starting from the metal surface and moving outward towards the bulk electrolyte. The atomic length-scale gap, x_1, between the metal and solvent regions corresponds to the separation between the induced charges on the metal surface and the nearest solvent molecules. This gap is necessary to reduce the magnitude of the capacitance and bring it in agreement with the experimental value near the PZC. Next, x_2, is the distance of closest approach of the solvated electrolyte ions as described in the Gouy-Chapman-Stern model. Without x_2, the ionic response is much closer to the metal surface and exhibits an overall higher capacitance with broader humps. Note that *both* x_1 and x_2 are necessary to simultaneously capture the capacitance magnitude at PZC and width of the humps in agreement with experiment.

The remaining two features considered in Fig. 12(b) relate to the nonlinearity of the fluid response. Specifically, $\varepsilon(E)$ is the nonlinear dielectric response of water and mPB (modified Poisson-Boltzmann) constrains the density of electrolyte ions by enforcing a packing limit (see Section 4.1 and Fig. 9). Both features cause a reduction of the capacitance at potentials far from the PZC, due to saturation of the dielectric response in $\varepsilon(E)$ and the saturation of the ionic response in mPB. For the aqueous KPF_6 electrolyte considered here, the dielectric saturation is a much stronger effect than ion packing in mPB. The presence or absence of mPB does not significantly change the capacitance curves for common aqueous electrolytes due to the strong nonlinear dielectric response and the relatively small ionic sizes. For larger organic ions, as is typical in ionic liquids, packing effects are more important requiring mPB, even at potentials near the PZC. [173][11]

In summary, capturing electrochemical capacitance in agreement with experiment requires nonlinearity in both the solvent dielectric response and ionic response, and both x_1 and x_2 regions. Most solvation models currently in use ignore nonlinearity of the dielectric response (Table 1), which would lead to capacitance curves that exhibit a much broader hump than experiment and overestimate the charge on the electrode at potentials far from the PZC. Additionally, using the same cavity for solvent and ions, which amounts to assuming $x_2 = 0$ also leads to capacitance curves with the wrong shape. The nonlinear electrochemical soft-sphere (NESS) solvation model [65] incorporates all features discussed above and exhibits qualitative agreement with experiment. However, applying this solvation model in a DFT calculation introduces asymmetries not seen in experiment or the toy model above due to a variation in the location of the electrode-induced charge density with potential [174], effectively making x_1 vary with potential. Therefore, no solvation model currently captures electrochemical capacitance with the accuracy shown in Fig. 12, necessitating further developments in cavity parameterizations for metal electrodes.

4.6. Structured / cavity-less implicit solvation

The solvation models discussed above all invoke a cavity to represent the distribution of the solvent and electrolyte, and then treat the response of this fluid distribution. Even nonlocal solvation models like SaLSA [18] which capture atomic-scale structure in the response of the liquid still assume a cavity distribution of the fluid as a starting point for perturbatively capturing the liquid response. An alternative strategy to continuum solvation treats the fluid distribution as an independent variable and optimizes it based on the interaction of the fluid with the solute. Such approaches can capture features in the distribution of the fluid, such as shell structures in solvation with oscillations in the fluid density at the size scale of the

[10] All curves in Fig. 12(b) include nonlinearity in the ionic response at the Poisson-Boltzmann (or mPB) level, without which the capacitance would not even exhibit a minimum at the potential of zero charge.

[11] Ignoring dielectric nonlinearity can lead to the erroneous conclusion that packing effects dominate the saturation in the response. In particular previous studies have used incorrectly large ionic radii, amplifying the ion saturation effect [66].

solvent molecule. Rearrangement of fluid charge distribution also captures the response implicitly, thereby unifying response and cavity considerations from solvation models above into a single problem of self-consistently optimizing the equilibrium fluid density.

Two complementary approaches provide a pathway to determine the equilibrium fluid density with atomic-scale structure around a solute. Integral equation theories establish nonlocal integral equations on the fluid density based on correlation functions and interaction potentials of the liquid [175–180]. Briefly, these theories work with the Ornstein-Zernike relation,

$$g_{\alpha\beta}(\vec{r},\vec{r}') = \delta_{\alpha\beta} + c_{\alpha\beta}(\vec{r},\vec{r}') + \sum_{\gamma}\int \mathrm{d}\vec{R}\; c_{\alpha\gamma}(\vec{r},\vec{R})\left(g_{\gamma\beta}(\vec{R},\vec{r}') - \delta_{\gamma\beta}\right) N_{\beta}(\vec{r}'). \quad (17)$$

This connects the pair distribution function $g_{\alpha\beta}(\vec{r},\vec{r}')$, related to probability of finding atom type α at $\vec{r}$ given an atom of type β located at $\vec{r}'$, with the direct correlation function $c_{\alpha\beta}(\vec{r},\vec{r}')$, related to the second functional derivative of the free energy with respect to the densities $N_\alpha(\vec{r})$ and $N_\beta(\vec{r}')$ of each atom type in the fluid. These theories additionally require an approximate "closure" relation between $g_{\alpha\beta}$ and $c_{\alpha\beta}$ e.g., the Percus-Yevick or hypernetted chain approximation, typically derived from diagrammatic expansions of the partition function of the fluid [181]. The free energy can then be estimated from the equilibrium fluid densities and direct correlation functions obtained by solving the equations [182–184].

On the other hand, classical density functional theory minimizes a free energy functional of the fluid density

$$\Phi_{\mathrm{lq}} = \min_{\{N_\alpha(\vec{r})\}}\left[k_BT\sum_{\alpha}\int \mathrm{d}\vec{r} N_\alpha(\vec{r})(\ln N_\alpha(\vec{r}) - 1 - \mu_\alpha) + \Phi_{\mathrm{ex}}[\{N_\alpha(\vec{r})\}]\right] \quad (18)$$

to simultaneously find the equilibrium free energy Φ_{lq} and fluid density profile N_α (density of atom type α). The first term is the exact non-interacting free energy of the fluid, while the second term Φ_{ex} is the excess functional that accounts for interactions, analogous to exchange-correlation functionals in electronic DFT. Classical DFT is exact in principle [185], but require approximation of the excess functionals in practical calculations for real liquids [114, 138]. Formally, integral equation theories may also be viewed as a pathway to approximate the free energy functional of classical DFT. In practice, integral equation theories typically yield more accurate density profiles, while classical DFT generally produces more accurate free energies.

Both approaches can be combined with DFT calculations of a solute or electrode to achieve a structured or cavity-less technique for implicit solvation. For example, integral equation theories in the reduced interaction-site model (RISM) framework [186, 187] have been combined with the electrostatic screening medium (ESM) [63] technique for DFT solvation in the ESM-RISM approach [67]. Classical DFT of solvents and electronic DFT of solutes combine together in joint density-functional theory (JDFT) of the solvated system [147, 188, 189]. Formally both such approaches can be summarized within the JDFT framework of minimizing a combined free energy functional of the solvated system,

$$\Phi_{\mathrm{JDFT}}[n,\{N_\alpha\}] = A_{\mathrm{HK}}[n] + \Phi_{\mathrm{lq}}[\{N_\alpha\}] + \Delta\Phi[n,\{N_\alpha\}]. \quad (19)$$

The first term is the Hohenberg-Kohn electronic functional in terms of the electron density $n(\vec{r})$ alone, the second term is the classical DFT liquid functional discussed above, and the final term is a coupling functional capturing interactions between the electronic and fluid systems. In practice, JDFT approaches directly approximate the free energy of the liquid and coupling terms as functionals of the densities [147, 188], while integral equation solvation approaches approximate the coupling based on interaction potentials (e.g. pair potentials) between solute and solvent atoms [67].

Solvation approaches which capture liquid structure may provide a level of solvation intermediate in accuracy and computational cost between conventional implicit models and explicit molecular dynamics techniques (Fig. 4). At present, these techniques need further work in developing stable and accurate free energy functionals for electrolytes (in addition to pure solvents), and algorithms to efficiently optimize the free energy or self-consistently determine the fluid densities.

5. Conclusions and outlook

In this review, we have described the diversity of methods used in *ab initio* electrochemical modeling, from the simplest methods with no solvent or electrolyte, to continuum, to full AIMD of solvent and electrolyte. We have discussed the fundamental challenges of electrochemical modeling for atomistic-level computation, namely the relatively long range of the electric fields and the need to describe thermodynamics of liquid solvent and electrolyte.

All explicit and implicit electrolyte implementations approximate interfacial physics, compromising between computational expense and accuracy. While no perfect method exists yet, both classes of methods have recently made significant progress towards describing the interface. The newest generation of continuum models have evolved to include the saturation of the dielectric response with electric field, and AIMD methodology has developed over the past decade to more accurately identify the applied potential in a given simulation.

However, challenges remain, especially in accessing longer length scales. Challenges in implicit solvation focus on capturing the capacitance of the interfacial region, and defining the near-surface region boundary. In explicit DFT

solvation, challenges include reducing computational expense and designing computations in the grand canonical ensemble. In classical explicit solvation, preserving electronic structure information, and properly handling charge transfer and polarization at large length-scales remain as unsolved challenges. Machine learning is rapidly changing computational science, and incipient fields such as machine-learned force fields and novel electronic structure approximations may hold the key to addressing these challenges. Continued methods development on multiple fronts is needed to capitalize on these opportunities, and to expand the application of computational electrochemical modeling.

Lastly, computational efforts are most useful in their relationship to experimental reality. Further experimental work to unravel atomically precise double layer structure [190], visualize electric fields, and evaluate capacitance [191] will provide new opportunities to test these models and parameterizations, and build new models.

References

[1] M. Pumera, Graphene-based nanomaterials for energy storage, Energy Environ. Sci. 4 (2011) 668–674. DOI:10.1039/C0EE00295J.

[2] N. Choi, Z. Chen, S. A. Freunberger, X. Ji, Y. Sun, K. Amine, G. Yushin, L. F. Nazar, J. Cho, P. G. Bruce, Challenges Facing Lithium Batteries and Electrical DoubleLayer Capacitors, Angew. Chemie 51 (2012) 9994–10024. DOI:10.1002/anie.201201429.

[3] F. Shen, X. Chen, P. Gao, G. Chen, Electrochemical removal of fluoride ions from industrial wastewater, Chem. Engg. Sci. 58 (2003) 987–993. DOI:10.1016/S0009-2509(02)00639-5.

[4] G. Chen, Electrochemical technologies in wastewater treatment, Sep. Purif. Tech. 38 (2004) 11–41. DOI:10.1016/j.seppur.2003.10.006.

[5] Y. Yavuz, A. S. Koparal, U. B. Ogutveren, Treatment of petroleum refinery wastewater by electrochemical methods, Desalination 258 (2010) 201–205. DOI:10.1016/j.desal.2010.03.013.

[6] N. R. Council, Research Opportunities in Corrosion Science and Engineering, The National Academies Press, Washington, DC, 2011. DOI:10.17226/13032.

[7] Y. Liu, D. Gokcen, U. Bertocci, T. P. Moffat, Self-Terminating Growth of Platinum Films by Electrochemical Deposition, Science 338 (6112) (2012) 1327–1330. DOI:10.1126/science.1228925.

[8] K. T. Butler, G. S. Gautam, P. Canepa, Designing interfaces in energy materials applications with first-principles calculations, npj Computational Materials 5. DOI:10.1038/s41524-019-0160-9.

[9] O. M. Magnussen, A. Gross, Toward an Atomic-Scale Understanding of Electrochemical Interface Structure and Dynamics, J. Am. Chem. Soc. 141 (2019) 47774790. DOI:10.1021/jacs.8b13188.

[10] A. Gross, Fundamental Challenges for Modeling Electrochemical Energy Storage Systems at the Atomic Scale, Topics Curr. Chem. (Z) 376 (2018) 17. DOI:10.1007/s41061-018-0194-3.

[11] J. L. Fattebert, F. Gygi, Firstprinciples molecular dynamics simulations in a continuum solvent, Int. J. Quantum Chem. 93 (2003) 139. DOI:10.1002/qua.10548.

[12] O. Andreussi, I. Dabo, N. Marzari, Revised Self-Consistent Continuum Solvation in Electronic-Structure Calculations, J. Chem. Phys 136 (2012) 064102. DOI:10.1063/1.3676407.

[13] D. Gunceler, K. Letchworth-Weaver, R. Sundararaman, K. Schwarz, T. Arias, The importance of nonlinear fluid response in joint density-functional theory studies of battery systems, Model. Simul. Mater. Sci. Eng. 21 (2013) 074005. DOI:10.1088/0965-0393/21/7/074005.

[14] K. Mathew, R. Sundararaman, K. Letchworth-Weaver, T. A. Arias, R. G. Hennig, Implicit Solvation Model for Density-Functional Study of Nanocrystal Surfaces and Reaction Pathways, J. Chem. Phys. 140 (2014) 084106. DOI:10.1063/1.4865107.

[15] O. Andreussi, G. Fisicaro, Continuum embeddings in condensed-matter simulations, Int. J. Quant. Chem. 119 (1) (2019) e25725. DOI:10.1002/qua.25725.

[16] J. A. Gauthier, S. Ringe, C. F. Dickens, A. J. Garza, A. T. Bell, M. Head-Gordon, J. K. Norskov, K. Chan, Challenges in Modeling Electrochemical Reaction Energetics with Polarizable Continuum Models, ACS Catal. 9 (2019) 920–931. DOI:10.1021/acscatal.8b02793.

[17] R. Sundararaman, W. Goddard, The Charge-Asymmetric Nonlocally-Determined Local-Electric (CANDLE) Solvation Model, J. Chem. Phys 142 (2015) 064107. DOI:10.1063/1.4907731.

[18] R. Sundararaman, K. Schwarz, K. Letchworth-Weaver, T. A. Arias, Spicing up continuum solvation models with SaLSA: the spherically-averaged liquid susceptibility ansatz, J. Chem. Phys. 142 (2015) 054102. DOI:10.1063/1.4906828.

[19] J. Sass, A surface physicist's view of electrochemistry, Vacuum 33 (1983) 741 – 751. DOI:10.1016/0042-207X(83)90602-4.

[20] D. Grahame, The Electrical Double Layer and the Theory of Electrocapillarity, Chem. Rev. 41 (1947) 441–501. DOI:10.1021/cr60130a002.

[21] M. Giesen, G. Beltramo, S. Dieluweit, J. Muller, H. Ibach, W. Schmickler, The thermodynamics of electrochemical annealing, Surf. Sci. 595 (2005) 127–137. DOI:10.1016/j.susc.2005.07.040.

[22] M. Nielsen, M. E. Bjorketun, M. H. Hansen, J. Rossmeisl, Towards first principles modeling of electrochemical electrode-electrolyte interfaces, Surf. Sci. 631 (2015) 2–7. DOI:10.1016/j.susc.2014.08.018.

[23] A. B. Anderson, R. Kotz, E. Yeager, Theory for CN and AgC vibrational frequency dependence on potential: cyanide on a silver electrode, Chem. Phys. Lett. 82 (1981) 130–134. DOI:10.1016/0009-2614(81)85122-6.

[24] A. B. Anderson, T. V. Albu, Ab initio determination of reversible potentials and activation energies for outer-sphere oxygen reduction to water and the reverse oxidation reaction, J. Am. Chem. Soc. 121 (1999) 11855–11863. DOI:10.1021/ja992735d.

[25] J. K. Norskov, J. Rossmeisl, A. Logadottir, L. Lindqvist, J. R. Kitchin, T. Bligaard, H. Jonsson, Origin of the Overpotential for Oxygen Reduction at a Fuel-Cell Cathode, J. Phys. Chem. B 108 (46) (2004) 17886–17892. DOI:10.1021/jp047349j.

[26] V. Tripkovic, M. E. Bjorketun, E. Skulason, J. Rossmeisl, Standard hydrogen electrode and potential of zero charge in density functional calculations, Phys. Rev. B 84 (2011) 115452. DOI:10.1103/PhysRevB.84.115452.

[27] G. S. Karlberg, J. Rossmeisl, J. K. Norskov, Estimations of electric field effects on the oxygen reduction reaction based on the density functional theory, Phys. Chem. Chem. Phys. 9 (2007) 5158–5161. DOI:10.1039/B705938H.

[28] L. D. Chen, M. Urushihara, K. Chan, J. K. Norskov, Electric Field Effects in Electrochemical CO2 Reduction, ACS Catalysis 6 (2016) 7133–7139. DOI:10.1021/acscatal.6b02299.

[29] H. Xiao, T. Cheng, W. A. Goddard, R. Sundararaman, Mechanistic Explanation of the pH Dependence and Onset Potentials for Hydrocarbon Products from Electrochemical Reduction of CO on Cu (111), Journal of the American Chemical Society 138 (2) (2016) 483–486. DOI:10.1021/jacs.5b11390.

[30] J. D. Goodpaster, A. T. Bell, M. Head-Gordon, Identification of Possible Pathways for C-C Bond Formation during Electrochemical Reduction of CO2: New Theoretical Insights from an Improved Electrochemical Model., J. Phys. Chem. Lett. 7 (2016) 1471. DOI:10.1021/acs.jpclett.6b00358.

[31] J. Bray, A. J. Hensley, G. Collinge, F. Che, Y. Wang, J.-S. McEwen, Modeling the adsorbate coverage distribution over a multi-faceted catalytic grain in the presence of an electric field: O/Fe from first principles, Catal. Today 312 (2018) 94–104. DOI:10.1016/j.cattod.2018.04.016.

[32] J. Filhol, M. Neurock, Elucidation of the Electrochemical Activation of Water over Pd by First Principles, Angew. Chem. Int. Ed. 45 (2006) 402–406. DOI:10.1002/anie.200502540.

[33] J. Rossmeisl, J. K. Norskov, C. D. Taylor, M. J. Janik, M. Neurock, Calculated Phase Diagrams for the Electrochemical Oxidation and Reduction of Water over Pt(111), J. Phys. Chem. B 110 (2006) 21833–21839. DOI:10.1021/jp0631735.

[34] A. J. Bard, L. R. Faulkner, Electrochemical Methods: Fundamentals and Applications, Wiley, 2000.

[35] A. Naumovets, Y. Vedula, Surface diffusion of adsorbates, Surface Science Reports 4 (7) (1985) 365 – 434. DOI:10.1016/0167-5729(85)90007-X.

[36] J. D. Roth, M. J. Weaver, Role of the Double-Layer Cation on the Potential-Dependent Stretching Frequencies and Binding Geometries of Carbon Monoxide at Platinum-Nonaqueous Interfaces, Langmuir 8 (1992) 1451–1458. DOI:10.1021/la00041a034.

[37] S. Wasileski, M. Koper, M. Weaver, Field-Dependent Electrode–Chemisorbate Bonding:Sensitivity of Vibrational Stark Effect and Binding Energetics to Nature of Surface Coordination, J. Am. Chem. Soc. 124 (2002) 2796–2805. DOI:10.1021/ja012200w.

[38] A. Ge, P. Videla, G. Lee, B. Rudshteyn, J. Song, C. Kubiak, V. Batista, T. Lian, Interfacial Structure and Electric Field Probed by in Situ Electrochemical Vibrational Stark Effect Spectroscopy and Computational Modeling, J. Phys. Chem. C 121 (2017) 18674–18682. DOI:10.1021/acs.jpcc.7b05563.

[39] J. Patrow, S. Sorenson, J. Dawlaty, Direct Spectroscopic Measurement of Interfacial Electric Fields near an Electrode under Polarizing or Current-Carrying Conditions, J. Phys. Chem. C 121 (2017) 11585–11592. DOI:10.1021/acs.jpcc.7b03134.

[40] R. Sundararaman, M. C. Figueiredo, M. Koper, K. A. Schwarz, Electrochemical capacitance of CO-terminated Pt (111) is dominated by CO-solvent gap, J. Phys. Chem. Lett. 8 (2017) 5344–5348. DOI:10.1021/acs.jpclett.7b02383.

[41] M. C.Figueiredo, D. Hiltrop, R. Sundararaman, K. A.Schwarz, M. T.M.Koper, Absence of diffuse double layer effect on the vibrational properties and oxidation of chemisorbed carbon monoxide on a Pt(111) electrode, Electrochimica Acta 281 (2018) 127 – 132. DOI:10.1016/j.electacta.2018.05.152.

[42] O. Stern, The Theory of the Electrolytic Double Shift, Z. Elektrochem. Angew. Phys. Chem. 30 (1924) 508–516. DOI:10.1002/bbpc.192400182.

[43] E. Skulason, G. S. Karlberg, J. Rossmeisl, T. Bligaard, J. Greeley, H. Jonsson, J. K. Norskov, Density functional theory calculations for the hydrogen evolution reaction in an electrochemical double layer on the Pt(111) electrode, Phys. Chem. Chem. Phys. 9 (2007) 3241–3250. DOI:10.1039/B700099E.

[44] J. Rossmeisl, E. Skulason, M. Bjorketun, V. Tripkovic, J. K. Norskov, Modeling the electrified solid-liquid interface, Chem. Phys. Lett. 466 (2008) 68–71. DOI:10.1016/j.cplett.2008.10.024.

[45] J. Cheng, M. Sprik, Alignment of electronic energy levels at electrochemical interfaces, Phys. Chem. Chem. Phys. 14 (2012) 11245–11267. DOI:10.1039/C2CP41652B.

[46] J.-B. Le, J. Cheng, Modeling electrochemical interfaces from ab initio molecular dynamics: water adsorption on metal surfaces at potential of zero charge, Current Opin. Electrochem. 19 (2020) 129–136. DOI:10.1016/j.coelec.2019.11.008.

[47] C. Zhan, D.-e. Jiang, Contribution of Dielectric Screening to the Total Capacitance of Few-Layer Graphene Electrodes, J. Phys. Chem. Lett. 7 (2016) 789–794. DOI:10.1021/acs.jpclett.6b00047.

[48] J. A. Gauthier, C. F. Dickens, H. H. Heenen, S. Vijay, S. Ringe, K. Chan, Unified Approach to Implicit and Explicit Solvent Simulations of Electrochemical Reaction Energetics, J. Chem. Theory Comput. 15 (2019) 6895–6906. DOI:10.1021/acs.jctc.9b00717.

[49] C. Zhan, P. Zhang, S. Dai, D.-e. Jiang, Boron Supercapacitors, ACS Energy Lett. 1 (6) (2016) 1241–1246. DOI:10.1021/acsenergylett.6b00483.

[50] Y. Gründer, D. Kaminski, F. Golks, K. Krug, J. Stettner, O. M. Magnussen, A. Franke, J. Stremme, E. Pehlke, Reversal of chloride-induced Cu(001) subsurface buckling in the electrochemical environment: An in situ surface x-ray diffraction and density functional theory study, Phys. Rev. B 81 (2010) 174114. DOI:10.1103/PhysRevB.81.174114.

[51] M. Saracino, P. Broekmann, K. Gentz, M. Becker, H. Keller, F. Janetzko, T. Bredow, K. Wandelt, H. Dosch, Surface relaxation phenomena at electrified interfaces: Revealing adsorbate, potential, and solvent effects by combined x-ray diffraction, STM and DFT studies, Phys. Rev. B 79 (2009) 115448. DOI:10.1103/PhysRevB.79.115448.

[52] A. Michaelides, A. Alavi, D. A. King, Different Surface Chemistries of Water on Ru0001: From Monomer Adsorption to Partially Dissociated Bilayers, J. Am. Chem. Soc. 125 (2003) 2746–2755. DOI:10.1021/ja028855u.

[53] S. Meng, E. G. Wang, S. Gao, Water adsorption on metal surfaces: A general picture from density functional theory studies,

Phys. Rev. B 69 (2004) 195404.
DOI:10.1103/PhysRevB.69.195404.

[54] S. Sakong, A. Gross, The electric double layer at metal-water interfaces revisited based on a charge polarization scheme, J. Chem. Phys. 149 (2018) 084705.
DOI:10.1063/1.5040056.

[55] J. Le, M. Iannuzzi, A. Cuesta, J. Cheng, Determining Potentials of Zero Charge of Metal Electrodes versus the Standard Hydrogen Electrode from Density-Functional-Theory-Based Molecular Dynamics, Phys. Rev. Lett. 119 (2017) 016801.
DOI:10.1103/PhysRevLett.119.016801.

[56] L. D. Chen, M. Bajdich, J. M. P. Martirez, C. M. Krauter, J. A. Gauthier, E. A. Carter, A. C. Luntz, K. Chan, J. K. Norskov, Understanding the apparent fractional charge of protons in the aqueous electrochemical double layer, Nature Commun. 9 (2018) 1–8.
DOI:10.1038/s41467-018-05511-y.

[57] A. Baskin, D. Prendergast, Exploring chemical speciation at electrified interfaces using detailed continuum models, J. Chem. Phys. 150 (2019) 041725.
DOI:10.1063/1.5058159.

[58] A. Baskin, D. Prendergast, Improving Continuum Models to Define Practical Limits for Molecular Models of Electrified Interfaces, J. Electrochem. Soc. 164 (2017) E3438–E3447.
DOI:10.1149/2.0461711jes.

[59] R. Sundararaman, W. A. Goddard III, T. A. Arias, Grand Canonical Electronic Density-Functional Theory: Algorithms and Applications to Electrochemistry, J. Chem. Phys. 146 (2017) 114104.
DOI:10.1063/1.4978411.

[60] J. Filhol, M. Neurock, Elucidation of the Electrochemical Activation of Water over Pd by First Principles, Angew. Chem. Int. Ed. 45 (2006) 402–406.
DOI:10.1002/anie.200502540.

[61] C. D. Taylor, S. A. Wasileski, J.-S. Filhol, , M. Neurock, First principles reaction modeling of the electrochemical interface: Consideration and calculation of a tunable surface potential from atomic and electronic structure, Phys. Rev. B 73 (2006) 165402.
DOI:10.1103/PhysRevB.73.165402.

[62] J. Zhao, C. T. Chan, , J. G. Che, Effects of an electric field on a water bilayer on Ag(111), Phys. Rev. B 75 (2007) 085435.
DOI:10.1103/PhysRevB.75.085435.

[63] M. Otani, O. Sugino, First-principles calculations of charged surfaces and interfaces: A plane-wave nonrepeated slab approach, Phys. Rev. B 73 (2006) 115407.
DOI:10.1103/PhysRevB.73.115407.

[64] Y. J. Feng, K. P. Bohnen, C. T. Chan, First-principles studies of Au(100)-hex reconstruction in an electrochemical environment, Phys. Rev. B 72 (2005) 125401.
DOI:10.1103/PhysRevB.72.125401.

[65] R. Sundararaman, K. Letchworth-Weaver, K. Schwarz, Improving accuracy of electrochemical capacitance and solvation energetics in first-principles calculations, J. Chem. Phys. 148 (2018) 144105.
DOI:10.1063/1.5024219.

[66] F. Nattino, M. Truscott, N. Marzari, O. Andreussi, Continuum models of the electrochemical diffuse layer in electronic-structure calculations, J. Chem. Phys. 150 (2019) 041722.
DOI:10.1063/1.5054588.

[67] S. Nishihara1, M. Otani, Hybrid solvation models for bulk, interface, and membrane: Reference interaction site methods coupled with density functional theory, Phys. Rev.B 96 (2017) 115429.
DOI:10.1103/PhysRevB.96.115429.

[68] O. Andreussi, N. Marzari, Electrostatics of solvated systems in periodic boundary conditions, Phys. Rev. B 90 (2014) 245101.
DOI:10.1103/PhysRevB.90.245101.

[69] J. F. Janak, Proof that $\partial E/\partial n_i = \epsilon$ in density-functional theory, Phys. Rev. B 18 (1978) 7165–7168.
DOI:10.1103/PhysRevB.18.7165.

[70] K. Letchworth-Weaver, T. A. Arias, Joint Density Functional Theory of the Electrode-Electrolyte Interface: Application to Fixed Electrode Potentials, Interfacial Capacitances, and Potentials of Zero Charge, Phys. Rev. B 86 (2012) 075140.
DOI:10.1103/PhysRevB.86.075140.

[71] S. Trasatti, The concept and physical meaning of absolute electrode potential: A Reassessment, J. Electroanal. Chem. 139 (1982) 1–13.
DOI:10.1016/0022-0728(82)85100-0.

[72] S. Trasatti, The absolute electrode potential: an explanatory note, Pure Appl. Chem. 58 (1986) 955–966.
DOI:10.1351/pac198658070955.

[73] S. Trasatti, The "absolute" electrode potentialthe end of the story, Electrochim. Acta 35 (1990) 269–271.
DOI:10.1016/0013-4686(90)85069-Y.

[74] S. Trasatti, Surface science and electrochemistry: concepts and problems, Surf. Sci. 335 (1995) 1–9.
DOI:10.1016/0039-6028(95)00446-7.

[75] J. Cheng, M. Sprik, Aligning electronic energy levels at the TiO2/H2O interface, Phys. Rev. B 82 (2010) 081406.
DOI:10.1103/PhysRevB.82.081406.

[76] N. Lespes, J.-S. Filhol, Using Implicit Solvent in Ab Initio Electrochemical Modeling: Investigating Li+/Li Electrochemistry at a Li/Solvent Interface, J. Chem. Theory Comput. 11 (7) (2015) 3375–3382.
DOI:10.1021/acs.jctc.5b00170.

[77] S. Sakong, M. Naderian, K. Mathew, R. G. Hennig, A. Gross, Density functional theory study of the electrochemical interface between a Pt electrode and an aqueous electrolyte using an implicit solvent method, J. Chem. Phys. 142 (2015) 234107.
DOI:10.1063/1.4922615.

[78] N. Bonnet, T. Morishita, O. Sugino, M. Otani, First-Principles Molecular Dynamics at a Constant Electrode Potential, Phys. Rev. Lett. 109 (2012) 266101.
DOI:10.1103/PhysRevLett.109.266101.

[79] S. Surendralal, M. Todorova, M. W. Finnis, J. Neugebauer, First-Principles Approach to Model Electrochemical Reactions: Understanding the Fundamental Mechanisms behind Mg Corrosion, Phys. Rev. Lett. (2018) 246801DOI:10.1103/PhysRevLett.120.246801.

[80] M. Head-Gordon, J. C. Tully, Molecular dynamics with electronic frictions, J. Chem. Phys. 103 (1995) 10137.
DOI:10.1063/1.469915.

[81] W. Dou, J. E. Subotnik, Universality of electronic friction: Equivalence of von Oppen's nonequilibrium Green's function approach and the Head-Gordon-Tully model at equilibrium, Phys. Rev. B 96 (2017) 104305.
DOI:10.1103/PhysRevB.96.104305.

[82] P. Spiering, K. Shakouri, J. Behler, G.-J. Kroes, J. Meyer, Orbital-Dependent Electronic Friction Significantly Affects the Description of Reactive Scattering of N2 from Ru(0001), J. Phys. Chem. Lett. 10 (2019) 2957–2962.
DOI:10.1021/acs.jpclett.9b00523.

[83] S. E. Weitzner, I. Dabo, Quantum-continuum simulation of underpotential deposition at electrified metal-solution interfaces, npj Comput. Mater. 3.
DOI:10.1038/s41524-016-0004-9.

[84] S. Weitzner, I. Dabo, Voltage-dependent cluster expansion for electrified solid-liquid interfaces: Application to the elec-

trochemical deposition of transition metals, Phys. Rev. B 96 (2017) 205134.
DOI:10.1103/PhysRevB.96.205134.

[85] C. Adriaanse, J. Cheng, V. Chau, M. Sulpizi, J. VandeVondele, M. Sprik, Aqueous Redox Chemistry and the Electronic Band Structure of Liquid Water, J. Phys. Chem. Lett. 323 (2012) 3411–3415.
DOI:10.1021/jz3015293.

[86] T. A. Pham, D. Lee, E. Schwegler, G. Galli, Interfacial Effects on the Band Edges of Functionalized Si Surfaces in Liquid Water, J. Am. Chem. Soc. 136 (2014) 17071–17077.
DOI:10.1021/ja5079865.

[87] C. Fang, W.-F. Li, R. S. Koster, J. Klimes, A. van Blaaderen, M. A. van Huis, The accurate calculation of the band gap of liquid water by means of GW corrections applied to plane-wave density functional theory molecular dynamics simulations, Phys. Chem. Chem. Phys. 17 (2015) 365–375.
DOI:10.1039/C4CP04202F.

[88] T. A. Pham, C. Zhang, E. Schwegler, G. Galli, Probing the electronic structure of liquid water with many-body perturbation theory, Phys. Rev. B 89 (2014) 060202(R).
DOI:10.1103/PhysRevB.89.060202.

[89] J. Rossmeisl, A. Logadottir, J.K.Norskov, Electrolysis of water on (oxidized) metal surfaces, Chem. Phys. 319 (2005) 178–184.
DOI:10.1016/j.chemphys.2005.05.038.

[90] D. Strmcnik, D. F. van der Vliet, K.-C. Chang, V. Komanicky, K. Kodama, H. You, V. R. Stamenkovic, N. M. Markovi, Effects of Li+, K+, and Ba2+ Cations on the ORR at Model and High Surface Area Pt and Au Surfaces in Alkaline Solutions, J. Phys. Chem. Lett. 221 (2011) 2733–2736.
DOI:10.1021/jz201215u.

[91] X. Chen, D. I. T. McCrum, D. K. A. Schwarz, P. D. M. J. Janik, P. D. M. T. M. Koper, Coadsorption of Cations as the Cause of the Apparent pH Dependence of Hydrogen Adsorption on a Stepped Platinum SingleCrystal Electrode, Angew. Chem. Int. Ed. 56 (2017) 15025–15029.
DOI:10.1002/anie.201709455.

[92] V. Stamenkovic, K. C. Chou, G. A. Somorjai, P. N. Ross, N. M Markovic, Vibrational Properties of CO at the Pt(111)Solution Interface: the Anomalous Stark-Tuning Slope, J. Phys. Chem. B 109 (2005) 678–680.
DOI:10.1021/jp044802i.

[93] J. Le, A. Cuesta, J. Cheng, The structure of metal-water interface at the potential of zero charge from density functional theory-based molecular dynamics, J. Electroanal. Chem. 819 (2018) 87 – 94.
DOI:10.1016/j.jelechem.2017.09.002.

[94] D. Adams, Grand canonical ensemble Monte Carlo for a Lennard-Jones fluid, Molec. Phys. 29 (1975) 307–311.
DOI:10.1080/00268977500100221.

[95] S. Boinepalli, P. Attard, Grand canonical molecular dynamics, J. Chem. Phys. 119 (2003) 12769.
DOI:10.1063/1.1629079.

[96] C. Lo, B. Palmer, Alternative Hamiltonian for molecular dynamics simulations in the grand canonical ensemble, J. Chem. Phys. 102 (1995) 925.
DOI:10.1063/1.469159.

[97] T. Cagin, B. M. Pettitt, Grand Molecular Dynamics: A Method for Open Systems, Molecular Simulation 6 (1991) 5–26.
DOI:10.1080/08927029108022137.

[98] M. H. Hansen, J. Rossmeisl, pH in Grand Canonical Statistics of an Electrochemical Interface, J. Phys. Chem. C 120 (2016) 29135–29143.
DOI:10.1021/acs.jpcc.6b09019.

[99] J. VandeVondele, The influence of temperature and density functional models in ab initio molecular dynamics simulation of liquid water, J. Chem. Phys. 122 (2005) 014515.
DOI:10.1063/1.1828433.

[100] M. J. Gillan, D. Alfe, A. Michaelides, Perspective: How good is DFT for water?, J. Chem. Phys. 144 (2016) 130901.
DOI:10.1063/1.4944633.

[101] H. Lin, D. G. Truhlar, QM/MM: what have we learned, where are we, and where do we go from here?, Theor Chem Acc 117 (2007) 185–199.
DOI:10.1007/s00214-006-0143-z.

[102] Dohm, Spohr, Korth, Developing adaptive QM/MM computer simulations for electrochemistry, J Comput Chem. 38 (2017) 51–58.
DOI:10.1002/jcc.24513.

[103] L.-P. Wang, T. V. Voorhis, A Polarizable QM/MM Explicit Solvent Model for Computational Electrochemistry in Water, J. Chem. Theory Comput. 8 (2012) 610–617.
DOI:10.1021/ct200340x.

[104] Z. Rinkevicius, X. Li, J. A. R. Sandberg, K. V. Mikkelsen, H. Agren, A Hybrid Density Functional Theory/Molecular Mechanics Approach for Linear Response Properties in Heterogeneous Environments, J. Chem. Theory Comput. 10 (2014) 989–1003.
DOI:10.1021/ct400897s.

[105] D. Golze, M. Iannuzzi, M.-T. Nguyen, D. Passerone, J. Hutter, Simulation of Adsorption Processes at Metallic Interfaces: An Image Charge Augmented QM/MM Approach, J. Chem. Theory Comput. 9 (2013) 5086–5097.
DOI:10.1021/ct400698y.

[106] H. J. C. Berendsen, J. R. Grigera, T. P. Straatsma, The missing term in effective pair potentials, J. Phys. Chem. 91 (1987) 6269.
DOI:10.1021/j100308a038.

[107] W. L. Jorgensen, J. Chandrasekhar, J. D. Madura, R. W. Impey, M. L. Klein, Comparison of simple potential functions for simulating liquid water, J. Chem. Phys. 79 (1983) 926.
DOI:10.1063/1.445869.

[108] J. L. F. Abascal, C. Vega, A general purpose model for the condensed phases of water: TIP4P/2005, J. Chem. Phys. 123 (2005) 234505.
DOI:10.1063/1.2121687.

[109] T. A. Halgren, W. Damm, Polarizable force fields, Current Opin. Struct. Bio. 11 (2) (2001) 236 – 242.
DOI:10.1016/S0959-440X(00)00196-2.

[110] S. W. Rick, S. J. Stuart, B. J. Berne, Dynamical fluctuating charge force fields: Application to liquid water, J. Chem. Phys. 101 (1994) 6141.
DOI:10.1063/1.468398.

[111] G. R. Medders, V. Babin, F. Paesani, Development of a First-Principles Water Potential with Flexible Monomers. III. Liquid Phase Properties, J. Chem. Theory Comput. 108 (2014) 2906–2910.
DOI:10.1021/ct5004115.

[112] L.-P. Wang, T. Head-Gordon, J. W. Ponder, P. Ren, J. D. Chodera, P. K. Eastman, T. J. Martinez, V. S. Pande, Systematic Improvement of a Classical Molecular Model of Water, J. Phys. Chem. B 117 (2013) 9956–9972.
DOI:10.1021/jp403802c.

[113] S. Naserifar, W. A. Goddard, Liquid water is a dynamic polydisperse branched polymer, Proc. Nat. Acad. Sci. 116 (6) (2019) 1998–2003.
DOI:10.1073/pnas.1817383116.

[114] R. Sundararaman, K. Letchworth-Weaver, T. A. Arias, A Recipe for Free-Energy Functionals of Polarizable Molecular

Fluids, J. Chem. Phys. 140 (2014) 144504.
DOI:10.1063/1.4870653.

[115] I. S. Joung, T. E. Cheatham, Determination of Alkali and Halide Monovalent Ion Parameters for Use in Explicitly Solvated Biomolecular Simulations, J. Phys. Chem. B 112 (30) (2008) 9020–9041.
DOI:10.1021/jp8001614.

[116] H. Sun, COMPASS: An ab Initio Force-Field Optimized for Condensed-Phase ApplicationsOverview with Details on Alkane and Benzene Compounds, J. Phys. Chem. B 102 (38) (1998) 7338–7364.
DOI:10.1021/jp980939v.

[117] A. D. MacKerell, D. Bashford, M. Bellott, R. L. Dunbrack, J. D. Evanseck, M. J. Field, S. Fischer, J. Gao, H. Guo, S. Ha, D. Joseph-McCarthy, L. Kuchnir, K. Kuczera, F. T. K. Lau, C. Mattos, S. Michnick, T. Ngo, D. T. Nguyen, B. Prodhom, W. E. Reiher, B. Roux, M. Schlenkrich, J. C. Smith, R. Stote, J. Straub, M. Watanabe, J. Wiorkiewicz-Kuczera, D. Yin, M. Karplus, All-Atom Empirical Potential for Molecular Modeling and Dynamics Studies of Proteins, J. Phys. Chem. B 102 (18) (1998) 3586–3616.
DOI:10.1021/jp973084f.

[118] W. D. Cornell, P. Cieplak, C. I. Bayly, I. R. Gould, K. M Merz, D. M. Ferguson, D. C. Spellmeyer, T. Fox, J. W. Caldwell, P. A. Kollman, A Second Generation Force Field for the Simulation of Proteins, Nucleic Acids, and Organic Molecules, J. Am. Chem. Soc. 117 (19) (1995) 5179–5197.
DOI:10.1021/ja00124a002.

[119] A. K. Rappe, C. J. Casewit, K. S. Colwell, I. Goddard, W. A., W. M. Skiff, UFF, a Full Periodic Table Force Field for Molecular Mechanics and Molecular Dynamics Simulations, J. Am. Chem. Soc. 114 (1992) 10024–10035.
DOI:10.1021/ja00051a040.

[120] D. W. Brenner, O. A. Shenderova, J. A. Harrison, S. J. Stuart, B. Ni, S. B. Sinnott, A second-generation reactive empirical bond order (REBO) potential energy expression for hydrocarbons, J. Phys.: Cond. Matt. 14.
DOI:10.1088/0953-8984/14/4/312.

[121] T. Liang, T.-R. Shan, Y.-T. Cheng, B. D. Devine, M. Noordhoek, Y. Li, Z. Lu, S. R. Phillpot, S. B. Sinnott, Classical atomistic simulations of surfaces and heterogeneous interfaces with the charge-optimized many body (COMB) potentials, Mater. Sci. Eng.: R: Reports 74 (2013) 255–279.
DOI:10.1016/j.mser.2013.07.001.

[122] T. P. Senftle, S. Hong, M. M. Islam, S. B. Kylasa, Y. Zheng, Y. K. Shin, C. Junkermeier, R. Engel-Herbert, M. J. Janik, H. M. Aktulga, T. Verstraelen, A. Grama, A. C. T. van Duin, The ReaxFF reactive force-field: development, applications and future directions, npj Comput. Mater. 2 (2016) 15011.
DOI:10.1038/npjcompumats.2015.11.

[123] S. G. Moore, D. R. Wheeler, Chemical potential perturbation: A method to predict chemical potentials in periodic molecular simulations, J. Chem. Phys. 134 (11) (2011) 114514.
DOI:10.1063/1.3561865.

[124] J. Behler, M. Parrinello, Generalized Neural-Network Representation of High-Dimensional Potential-Energy Surfaces, Phys. Rev. Lett. 98 (2007) 146401.
DOI:10.1103/PhysRevLett.98.146401.

[125] J. Behler, Perspective: Machine learning potentials for atomistic simulations, J. Chem. Phys. 145 (2016) 170901.
DOI:10.1063/1.4966192.

[126] Y.-J. Zhang, A. Khorshidi, G. Kastlunger, A. A. Peterson, The potential for machine learning in hybrid QM/MM calculations, J. Chem. Phys. 148 (2018) 241740.
DOI:10.1063/1.5029879.

[127] V. Quaranta, J. Behler, M. Hellstrom, Structure and Dynamics of the Liquid-Water/Zinc-Oxide Interface from Machine Learning Potential Simulations, J. Phys. Chem. C 123 (2019) 1293–1304.
DOI:10.1021/acs.jpcc.8b10781.

[128] A. P. Bartok, M. C. Payne, R. Kondor, G. Csanyi, Gaussian Approximation Potentials: The Accuracy of Quantum Mechanics, without the Electrons, Phys. Rev. Lett. 104 (2010) 136403.
DOI:10.1103/PhysRevLett.104.136403.

[129] A. Grisafi, M. Ceriotti, Incorporating long-range physics in atomic-scale machine learning (2019).
DOI:10.1063/1.5128375.

[130] S. A. Ghasemi, A. Hofstetter, S. Saha, S. Goedecker, Interatomic potentials for ionic systems with density functional accuracy based on charge densities obtained by a neural network, Phys. Rev. B 92 (2015) 045131.
DOI:10.1103/PhysRevB.92.045131.

[131] P. Goyal, H.-J. Qian, S. Irle, X. Lu, D. Roston, T. Mori, M. Elstner, Q. Cui, Molecular Simulation of Water and Hydration Effects in Different Environments: Challenges and Developments for DFTB Based Models, J. Phys. Chem. B 118 (2014) 11007–11027.
DOI:10.1021/jp503372v.

[132] S. Rossbach, C. Ochsenfeld, Influence of Coupling and Embedding Schemes on QM Size Convergence in QM/MM Approaches for the Example of a Proton Transfer in DNA, J. Chem. Theory Comput. 133 (2017) 1102–1107.
DOI:10.1021/acs.jctc.6b00727.

[133] T. Loytynoja, X. Li, K. Jankala, Z. Rinkevicius, H. Agren, Quantum mechanics capacitance molecular mechanics modeling of core-electron binding energies of methanol and methyl nitrite on Ag(111) surface, J. Chem. Phys. 145 (2016) 024703.
DOI:10.1063/1.4956449.

[134] S. N. Steinmann, P. FleuratLessard, A. W. Gotz, C. Michel, R. F. de Morais, P. Sautet, Molecular mechanics models for the image charge, a comment on including image charge effects in the molecular dynamics simulations of molecules on metal surfaces, J. Comput. Chem. 38.
DOI:10.1002/jcc.24861.

[135] F. Iori, S. Corni, Including image charge effects in the molecular dynamics simulations of molecules on metal surfaces, J. Comput. Chem. 29.
DOI:10.1002/jcc.20928.

[136] J. I. Siepmann, M. Sprik, Influence of surface topology and electrostatic potential on water/electrode systems, J. Chem. Phys. 102 (1995) 511.
DOI:10.1063/1.469429.

[137] T. Markovich, D. Andelman, R. Podgornik, Charged Membranes: Poisson-Boltzmann theory, DLVO paradigm and beyond, in: C. Safinya, J. Radler (Eds.), Handbook of Lipid Membranes: Molecular, Functional, and Materials Aspects, Taylor & Francis, 2016, Ch. 9.

[138] R. Sundararaman, T. Arias, Efficient classical density-functional theories of rigid-molecular fluids and a simplified free energy functional for liquid water, Comp. Phys. Comm. 185 (2014) 818.
DOI:10.1016/j.cpc.2013.11.013.

[139] D. J. Griffiths, Introduction to electrodynamics; 4th ed., Pearson, 2013.

[140] J. G. Kirkwood, The Dielectric Polarization of Polar Liquids, J. Chem. Phys 7 (1939) 911.
DOI:10.1063/1.1750343.

[141] J. K. Staffa, L. Lorenz, M. Stolarski, D. H. Murgida, I. Zebger, T. Utesch, J. Kozuch, P. Hildebrandt, Determination of the Lo-

cal Electric Field at Au/SAM Interfaces Using the Vibrational Stark Effect, J. Phys. Chem. C 121 (2017) 22274–22285. DOI:10.1021/acs.jpcc.7b08434.

[142] S. D. Fried, S. Bagchi, S. G. Boxer, Extreme electric fields power catalysis in the active site of ketosteroid isomerase, Science 346 (2014) 1510–1514. DOI:10.1126/science.1259802.

[143] J. Tomasi, B. Mennucci, R. Cammi, Quantum Mechanical Continuum Solvation Models, Chem. Rev. 105 (2005) 2999. DOI:10.1021/cr9904009.

[144] J. Tomasi, M. Persico, Molecular-Interactions in Solution - an Overview of Methods Based on Continuous Distributions of the Solvent, Chem. Rev. 94 (1994) 20272094. DOI:10.1021/cr00031a013.

[145] J. L. Fattebert, F. Gygi, Density functional theory for efficient ab initio molecular dynamics simulations in solution, J. Comput. Chem. 23 (2002) 662. DOI:10.1002/jcc.10069.

[146] G. Scalmania, M. J. Frisch, Continuous surface charge polarizable continuum models of solvation. I. General formalism, J. Chem. Phys. 132 (2010) 114110. DOI:10.1063/1.3359469.

[147] S. A. Petrosyan, J.-F. Briere, D. Roundy, T. A. Arias, Joint density-functional theory for electronic structure of solvated systems, Phys. Rev. B 75 (2007) 205105. DOI:10.1103/PhysRevB.75.205105.

[148] R. Sundararaman, K. Schwarz, Evaluating Continuum Solvation Models for the Electrode-Electrolyte Interface: Challenges and Strategies for Improvement, J. Chem. Phys. 146 (2017) 084111. DOI:10.1063/1.4976971.

[149] C. Dupont, O. Andreussi, N. Marzari, Self-Consistent Continuum Solvation (SCCS): the Case of Charged Systems, J. Chem. Phys 139 (2013) 214110. DOI:10.1063/1.4832475.

[150] R. Sundararaman, D. Gunceler, T. A. Arias, Weighted-density functionals for cavity formation and dispersion energies in continuum solvation models, J. Chem. Phys. 141 (2014) 134105. DOI:10.1063/1.4896827.

[151] M. Truscott, O. Andreussi, Field-Aware Interfaces in Continuum Solvation, J. Phys. Chem. B 123 (2019) 3513–3524. DOI:10.1021/acs.jpcb.9b01363.

[152] A. V. Marenich, C. P. Kelly, J. D. Thompson, G. D. Hawkins, C. C. Chambers, D. J. Giesen, P. Winget, C. J. Cramer, D. G. Truhlar, Minnesota Solvation Database – version 2012, University of Minnesota, 2012.

[153] D. J. Tannor, B. Marten, R. Murphy, R. A. Friesner, D. Sitkoff, A. Nicholls, M. Ringnalda, W. A. Goddard, B. Honig, Accurate First Principles Calculation of Molecular Charge Distributions and Solvation Energies from Ab Initio Quantum Mechanics and Continuum Dielectric Theory, J. Am. Chem. Soc. 116 (1994) 11875–11882. DOI:10.1021/ja00105a030.

[154] B. Marten, K. Kim, C. Cortis, R. A. Friesner, R. B. Murphy, M. N. Ringnalda, D. Sitkoff, B. Honig, New Model for Calculation of Solvation Free Energies: Correction of Self-Consistent Reaction Field Continuum Dielectric Theory for Short-Range Hydrogen-Bonding Effects, J. Phys. Chem. 100 (1996) 11775–11788. DOI:10.1021/jp953087x.

[155] G. Fisicaro, L. Genovese, O. Andreussi, S. Mandal, N. N. Nair, N. Marzari, S. Goedecker, Soft-Sphere Continuum Solvation in Electronic-Structure Calculations, J. Chem. Theory Comput. 13 (2017) 3829–3845. DOI:10.1021/acs.jctc.7b00375.

[156] D. M. Huang, P. L. Geissler, D. Chandler, Scaling of Hydrophobic Solvation Free Energies, J. Phys. Chem. B 105 (2001) 6704. DOI:10.1021/jp0104029.

[157] R. A. Pierotti, A scaled particle theory of aqueous and nonaqueous solutions, Chem. Rev. 76 (1976) 717. DOI:10.1021/cr60304a002.

[158] C. Colominas, F. J. Luque, J. Teixido, M. Orozco, Cavitation contribution to the free energy of solvation.: Comparison of different formalisms in the context of MST calculations, Chem. Phys. 240 (1999) 253. DOI:10.1016/S0301-0104(98)00333-4.

[159] J. Langlet, P. Claverie, J. Caillet, A. Pullman, Improvements of the continuum model. 1. Application to the calculation of the vaporization thermodynamic quantities of nonassociated liquids, J. Phys. Chem. 92 (1988) 1617. DOI:10.1021/j100317a048.

[160] S. Grimme, Semiempirical GGAtype density functional constructed with a longrange dispersion correction, J. Comput. Chem 27 (2006) 1787. DOI:10.1002/jcc.20495.

[161] A. Tkatchenko, M. Scheffler, Accurate Molecular Van Der Waals Interactions from Ground-State Electron Density and Free-Atom Reference Data, Phys. Rev. Lett. 102 (2009) 073005. DOI:10.1103/PhysRevLett.102.073005.

[162] C. Amovilli, B. Mennucci, Self-Consistent-Field Calculation of Pauli Repulsion and Dispersion Contributions to the Solvation Free Energy in the Polarizable Continuum Model, J. Phys. Chem. B 101 (1997) 1051. DOI:10.1021/jp9621991.

[163] C. M. Gray, K. Saravanan, G. Wang, J. A. Keith, Quantifying solvation energies at solid/liquid interfaces using continuum solvation methods, Mol. Simul. 43 (2017) 420–427. DOI:10.1080/08927022.2016.1273525.

[164] A. V. Marenich, C. J. Cramer, D. G. Truhlar, Universal Solvation Model Based on Solute Electron Density and on a Continuum Model of the Solvent Defined by the Bulk Dielectric Constant and Atomic Surface Tensions, J. Phys. Chem. B 113 (2009) 6378. DOI:10.1021/jp810292n.

[165] C. Hille, S. Ringe, M. Deimel, C. Kunkel, W. Acree, K. Reuter, H. Oberhofer, Generalized molecular solvation in non-aqueous solutions by a single parameter implicit solvation scheme, J. Chem. Phys. 150 (2019) 041710. DOI:10.1063/1.5050938.

[166] R. Jinnouchi, A. Anderson, Electronic Structure Calculations of Liquid–Solid Interfaces: Combination of Density Functional Theory and Modified Poisson-Boltzmann Theory, Phys. Rev. B 77 (2008) 245417. DOI:10.1103/PhysRevB.77.245417.

[167] I. Dabo, Y. Li, N. Bonnet, N. Marzari, Ab Initio Electrochemical Properties of Electrode Surfaces, in: A. Wieckowski, J. Norskov (Eds.), Fuel Cell Science: Theory, Fundamentals, and Biocatalysis, Wiley, 2010, Ch. 13, pp. 415–431. DOI:10.1002/9780470630693.ch13.

[168] C. J. Cramer, D. G. Truhlar, General parameterized SCF model for free energies of solvation in aqueous solution, J.Am. Chem. Soc. 113 (1991) 8305. DOI:10.1021/ja00022a017.

[169] A. V. Marenich, R. M. Olson, C. P. Kelly, C. J. Cramer, D. G. Truhlar, Self-Consistent Reaction Field Model for Aqueous and Nonaqueous Solutions Based on Accurate Polarized Partial Charges, J. Chem. Theory Comput. (2007) 2011DOI: 10.1021/ct7001418.

[170] A. Fortunelli, J. Tomasi, The implementation of density functional theory within the polarizable continuum model for solvation, Chem. Phys. Lett. 231 (1994) 34. DOI:10.1016/0009-2614(94)01253-9.

[171] V. Barone, M. Cossi, J. Tomasi, A new definition of cavities for the computation of solvation free energies by the polarizable continuum model, J. Chem. Phys. 107 (1997) 3210. DOI:10.1063/1.474671.

[172] G. Valette, Double layer on silver single crystal electrodes in contact with electrolytes having anions which are slightly specifically adsorbed: Part II. The (100) face, J. Electroanal. Chem. Interf. Electrochem. 138 (1982) 37–54. DOI:10.1016/0022-0728(82)87126-X.

[173] M.V.Fedorov, N.Georgia, A.Kornyshev, Double layer in ionic liquids: The nature of the camel shape of capacitance, Electrochem. Commun. 12 (2010) 296–299. DOI:10.1016/j.elecom.2009.12.019.

[174] S. Amokrane, J. P. Badiali, Analysis of the Capacitance of the Metal–Solution Interface: Role of the Metal and the Metal–Solvent Coupling, in: Bockris (Ed.), Modern Aspects of Electrochemistry, Number 22, Springer, 1992, pp. 1–95. DOI:10.1007/978-1-4615-3376-4_1.

[175] A. Kovalenko, F. Hirata, Self-consistent description of a metal–water interface by the Kohn-Sham density functional theory and the three-dimensional reference interaction site model, J. Chem. Phys. 110 (20) (1999) 10095–10112. DOI:10.1063/1.478883.

[176] S. Gusarov, T. Ziegler, A. Kovalenko, Self-Consistent Combination of the Three-Dimensional RISM Theory of Molecular Solvation with Analytical Gradients and the Amsterdam Density Functional Package, J. Phys. Chem. A 110 (18) (2006) 6083–6090. DOI:10.1021/jp054344t.

[177] D. Casanova, S. Gusarov, A. Kovalenko, T. Ziegler, Evaluation of the SCF Combination of KS-DFT and 3D-RISM-KH; Solvation Effect on Conformational Equilibria, Tautomerization Energies, and Activation Barriers, J. Chem. Theory Comput. 3 (2) (2007) 458–476. DOI:10.1021/ct6001785.

[178] T. A. Wesolowski, A. Warshel, Frozen density functional approach for ab initio calculations of solvated molecules, J. Phys. Chem. 97 (30) (1993) 8050–8053. DOI:10.1021/j100132a040.

[179] T. Wesolowski, A. Warshel, Ab Initio Free Energy Perturbation Calculations of Solvation Free Energy Using the Frozen Density Functional Approach, J. Phys. Chem. 98 (20) (1994) 5183–5187. DOI:10.1021/j100071a003.

[180] J. W. Kaminski, S. Gusarov, T. A. Wesolowski, A. Kovalenko, Modeling Solvatochromic Shifts Using the Orbital-Free Embedding Potential at Statistically Mechanically Averaged Solvent Density, J. Phys. Chem. A 114 (20) (2010) 6082–6096. DOI:10.1021/jp100158h.

[181] J.-P. Hansen, I. R. McDonald, Chapter 4 - Distribution Function Theories, in: J.-P. Hansen, I. R. McDonald (Eds.), Theory of Simple Liquids (Fourth Edition), fourth edition Edition, Academic Press, Oxford, 2013, pp. 105 – 147. DOI:10.1016/B978-0-12-387032-2.00004-0.

[182] K. Kido, D. Yokogawa, H. Sato, A modified repulsive bridge correction to accurate evaluation of solvation free energy in integral equation theory for molecular liquids, J. Chem. Phys. 137 (2012) 024106. DOI:10.1063/1.4733393.

[183] M. Misin, M. V. Fedorov, D. S. Palmer, Communication: Accurate hydration free energies at a wide range of temperatures from 3D-RISM, J. Chem. Phys. 142 (9) (2015) 091105. DOI:10.1063/1.4914315.

[184] G. N. Chuev, M. Valiev, M. V. Fedotova, Integral Equation Theory of Molecular Solvation Coupled with Quantum Mechanical/Molecular Mechanics Method in NWChem Package, J. Chem. Theory Comput. 8 (4) (2012) 1246–1254. DOI:10.1021/ct2009297.

[185] N. D. Mermin, Thermal Properties of the Inhomogeneous Electron Gas, Phys. Rev. 137 (1965) A1441. DOI:10.1103/PhysRev.137.A1441.

[186] D. Chandler, J. McCoy, S. Singer, Density functional theory of nonuniform polyatomic systems. I. General formulation, J. Chem. Phys. 85 (1986) 5971. DOI:10.1063/1.451510.

[187] D. Chandler, J. McCoy, S. Singer, Density functional theory of nonuniform polyatomic systems. II. Rational closures for integral equations, J. Chem. Phys. 85 (1986) 5978. DOI:10.1063/1.451511.

[188] M. Plaza, X. Huang, J. Y. P. Ko, M. Shen, B. H. Simpson, J. Rodríguez-López, N. L. Ritzert, K. Letchworth-Weaver, D. Gunceler, D. G. Schlom, T. A. Arias, J. D. Brock, H. D. Abruña, Structure of the Photo-catalytically Active Surface of SrTiO3, Journal of the American Chemical Society 138 (25) (2016) 7816–7819. DOI:10.1021/jacs.6b03338.

[189] R. Sundararaman, K. Letchworth-Weaver, K. A. Schwarz, D. Gunceler, Y. Ozhabes, T. Arias, JDFTx: Software for joint density-functional theory, SoftwareX 6 (2017) 278 – 284. DOI:10.1016/j.softx.2017.10.006.

[190] Y. Liu, T. Kawaguchi, M. S. Pierce, V. Komanicky, H. You, Layering and Ordering in Electrochemical Double Layers, J. Phys. Chem. Lett. 9 (2018) 1265–1271. DOI:10.1021/acs.jpclett.8b00123.

[191] M. T. M. Koper, K. Ojha, N. Arulmozhi, D. Aranzales, Double layer of Pt(111)-aqueous electrolyte interface: Potential of Zero Charge and Anomalous Gouy-Chapman Screening, Angew. Chem. Int. Ed.DOI:10.1002/anie.201911929.